

1982

A study of the E.P.R. spectrum of potassium sulfate : copper(2+).

David John. Unwin
University of Windsor

Follow this and additional works at: <http://scholar.uwindsor.ca/etd>

Recommended Citation

Unwin, David John., "A study of the E.P.R. spectrum of potassium sulfate : copper(2+)." (1982). *Electronic Theses and Dissertations*. Paper 792.

This online database contains the full-text of PhD dissertations and Masters' theses of University of Windsor students from 1954 forward. These documents are made available for personal study and research purposes only, in accordance with the Canadian Copyright Act and the Creative Commons license—CC BY-NC-ND (Attribution, Non-Commercial, No Derivative Works). Under this license, works must always be attributed to the copyright holder (original author), cannot be used for any commercial purposes, and may not be altered. Any other use would require the permission of the copyright holder. Students may inquire about withdrawing their dissertation and/or thesis from this database. For additional inquiries, please contact the repository administrator via email (scholarship@uwindsor.ca) or by telephone at 519-253-3000ext. 3208.

CANADIAN THESES ON MICROFICHE

I.S.B.N.

THESES CANADIENNES SUR MICROFICHE



National Library of Canada
Collections Development Branch

Canadian Theses on
Microfiche Service

Ottawa, Canada
K1A 0N4

Bibliothèque nationale du Canada
Direction du développement des collections

Service des thèses canadiennes
sur microfiche

NOTICE

The quality of this microfiche is heavily dependent upon the quality of the original thesis submitted for microfilming. Every effort has been made to ensure the highest quality of reproduction possible.

If pages are missing, contact the university which granted the degree.

Some pages may have indistinct print especially if the original pages were typed with a poor typewriter ribbon or if the university sent us a poor photocopy.

Previously copyrighted materials (journal articles, published tests, etc.) are not filmed.

Reproduction in full or in part of this film is governed by the Canadian Copyright Act, R.S.C. 1970, c. C-30. Please read the authorization forms which accompany this thesis.

THIS DISSERTATION
HAS BEEN MICROFILMED
EXACTLY AS RECEIVED

AVIS

La qualité de cette microfiche dépend grandement de la qualité de la thèse soumise au microfilmage. Nous avons tout fait pour assurer une qualité supérieure de reproduction.

S'il manque des pages, veuillez communiquer avec l'université qui a conféré le grade.

La qualité d'impression de certaines pages peut laisser à désirer, surtout si les pages originales ont été dactylographiées à l'aide d'un ruban usé ou si l'université nous a fait parvenir une photocopie de mauvaise qualité.

Les documents qui font déjà l'objet d'un droit d'auteur (articles de revue, examens publiés, etc.) ne sont pas microfilmés.

La reproduction, même partielle, de ce microfilm est soumise à la Loi canadienne sur le droit d'auteur, SRC 1970, c. C-30. Veuillez prendre connaissance des formules d'autorisation qui accompagnent cette thèse.

LA THÈSE A ÉTÉ
MICROFILMÉE TELLE QUE
NOUS L'AVONS REÇUE

A STUDY OF THE E.P.R. SPECTRUM
OF $K_2SO_4 : Cu^{2+}$

by



David John Unwin

A Thesis
Submitted to the Faculty of Graduate Studies
through the Department of Physics in
Partial Fulfillment of the Requirements
for the Degree of Master of Science
at the University of Windsor

Windsor, Ontario

1982

ABSTRACT

The system $K_2SO_4:Cu^{2+}$ produces four sets of spectra and the previously uninvestigated weak set was studied by electron paramagnetic resonance methods.

The data were fitted to the spin Hamiltonian

$$H = S.g.H + S.A.I. + I.Q.I$$

using an exact diagonalization process and a multi-dimensional least squares method. The parameters were found to be (in crystallographic co-ordinates)

g _{xx}	g _{yy}	g _{zz}
2.5396±.0001	2.1296±.0001	2.0920±.0001
g _{xy}	g _{zx}	g _{zy}
0.1023±.0001	0.0347±.0001	0.0516±.0002
A x·10 ⁻⁴ cm ⁻¹	A _{yy}	A _{zz}
205.3±0.9	19.9± 5.6	38.5±4.0
A _{xy}	A _{zx}	A _{zy}
88.3±2.0	2.3±1.6	-36.9±4.5
Q _x ·10 ⁻⁴ cm ⁻¹	Q _y	
20.6±2	3.8±0.6	

Diagonalization of g and A tensors show that they are highly non-coincident. This is due to a very low symmetry environment of the paramagnetic impurity. Reasonable agreement with a previously suggested charge compensation mode was also found.



ACKNOWLEDGEMENTS

The author wishes to thank Dr. F. Holuj for his guidance during the work and Dr. M. Khan for x-ray crystallography enabling identification of axes.

TABLE OF CONTENTS

	Page
ABSTRACT	iii
ACKNOWLEDGEMENTS	v
LIST OF TABLES	viii
LIST OF FIGURES	ix
CHAPTER	
I. INTRODUCTION AND PURPOSE OF EXPERIMENT	1
II. THE CRYSTAL STRUCTURE OF K_2SO_4	2
III. THEORY	4
A. Electron Paramagnetic Resonance	4
B. The Divalent Copper Ion	6
C. The Complete Hamiltonian	7
D. The Spin Hamiltonian	9
IV. INSTRUMENTATION	12
A. K-Bond Spectrometer	12
(1) Klystron Stabilizer	12
(2) Microwave Circuit	14
(3) External Magnetic Field and Modulations	17
B. Proton Magnetometer	17
V. EXPERIMENTAL PROCEDURE	
(1) Crystal Orientation	18
(2) Measurement of Magnetic Field	26
(3) Measurement of Microwave Frequency	28
VI. DEVELOPMENT OF COMPUTER PROGRAM	29
A. The Method	29

B. The Flow Chart	34
C. Rate of Convergence	37
VII. DISCUSSION AND CONCLUSION	39
BIBLIOGRAPHY	48
APPENDIX 1. DATA	49
2. Identification of Crystallographic axes	51
3. Program used for calculating P(I)	52
4. STCM: Similarity Transform Converts Matrix Elements to New Basis	55
5. RTN 1: Main Subroutine	56
6. CEIGEN - Computes Eigenvalues and Eigenrectors of Hermitian Matrix (double precision complex)	63
7. DGMPRO: Matrix Multiplication of two general double precision matrices	64
8. Diagonalization of g and A tensor	65
VITA AUCTORIS	68

LIST OF TABLES

		Page
IV.	1 Rate of Convergence	37
VII.	1 Spectral Parameters	40

LIST OF FIGURES

		Page	
II.	1	Crystal Structure of K_2SO_4	3
IV.	1	Block Diagram of Spectrometer	13
IV.	3	Diagram of Microwave Detector and Balanced transformer	15
V.	1-3	Spectra along crystallographic axes	19, 20, 21
V.	4-6	Angular variation	23, 24, 25
V.	7	P.M.R. Probe	27
V.	8	P.M.R. Signal	28
VI.	1	Block diagram of Computer Program	35
VII.	1	Crystal Structure of K_2SO_4	42
VII.	3	Stereogram of g and A tensors	43

CHAPTER I
INTRODUCTION AND PURPOSE OF EXPERIMENT

Although the initial objective had been to study $\text{LiK}_2\text{SO}_4:\text{Cu}^{2+}$, obtaining samples proved to be difficult and $\text{K}_2\text{SO}_4:\text{Cu}^{2+}$ was investigated instead.

The course of searching for a crystal of LiK_2SO_4 with sufficient copper doping to produce strong electron paramagnetic resonance signals yielded crystals of K_2SO_4 with extremely strong signals.

Although the spectrum of $\text{K}_2\text{SO}_4:\text{Cu}^{2+}$ had previously been investigated by Abdulsabirov¹ and Freeman², these investigations left open the questions of non coincident g and A tensor and although Abdulsabirov¹ had evaluated three sets of spectra, the charge compensation mechanism they suggested left open the possibility of a fourth mechanism and a set of weak lines had not been investigated by 1 or 2.

The purpose of the investigation was to evaluate the spectrum of this weak set and to check agreement with both the charge compensation mechanism suggested by 1 and the non-coincidences reported by 2. For this purpose crystals containing a single isotope Cu^{63} were prepared thus yielding a greater resolution since the relaxation times (spin-lattice) at 77°K were such that the Cu^{63} and Cu^{65} lines overlapped.

CHAPTER II

THE CRYSTAL STRUCTURE OF K_2SO_4

X-ray studies ³ have shown that K_2SO_4 is orthorhombic with $a=7.456\text{\AA}$, $b=10.08\text{\AA}$, $c=5.776\text{\AA}$ and has space group $Pnam$, (D_{2n}^{16}).

Each unit cell contains 4 formula units and the SO_4 groups form groups of symmetry related tetrahedra.

A diagram of the crystal structure is shown in fig. II.1 with a box around the unit cell.

The crystals were grown from aqueous solution by slow evaporation at room temperature and doped with Cu^{63} during growth.

30

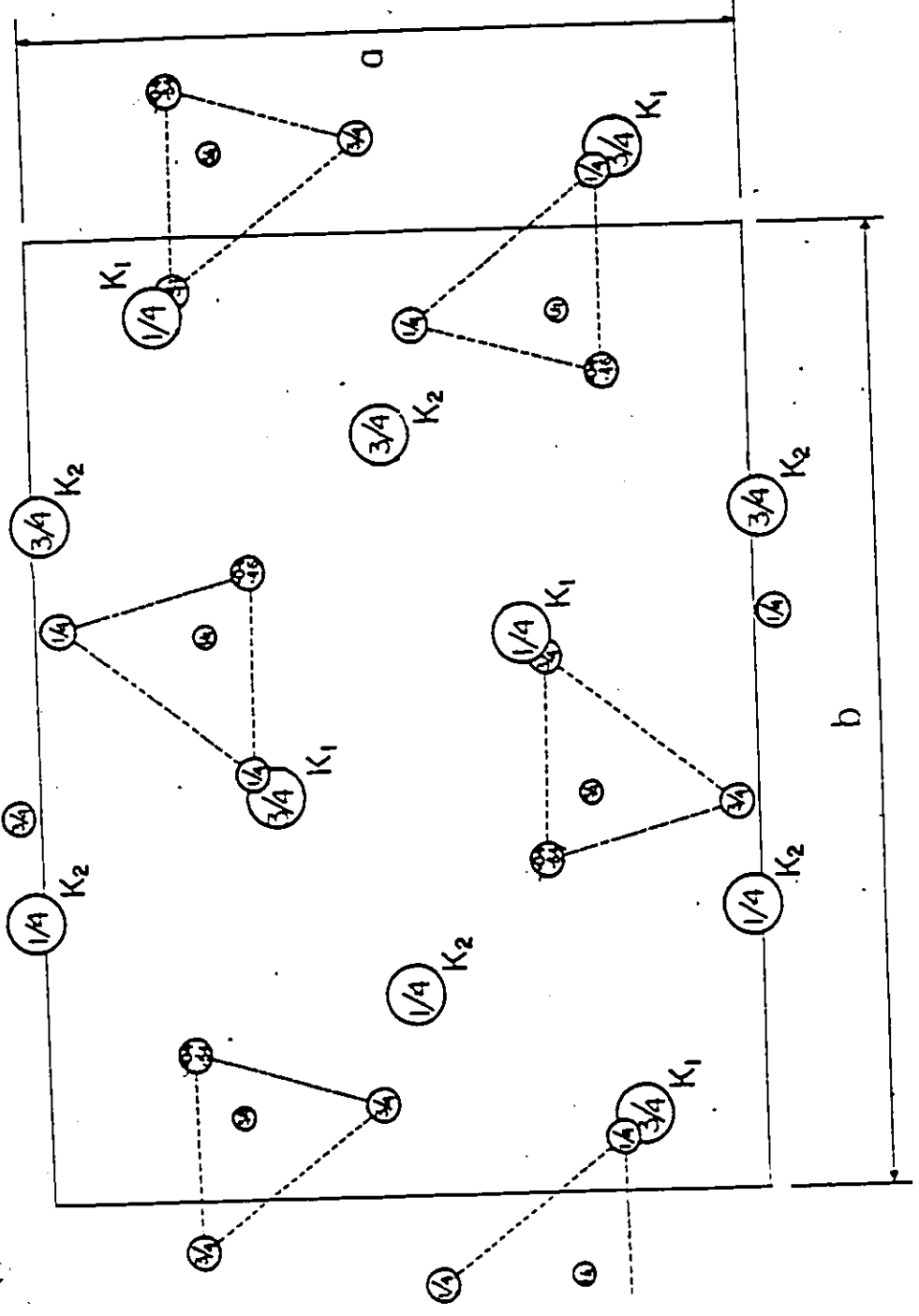


FIG II.1

CHAPTER III

THEORY

A. Electron Paramagnetic Resonance

This phenomenon was first reported by Zavoyskiy⁴ in 1945 and refers to the magnetic resonance of permanent magnetic dipole moments of electrons.

Paramagnetic centres may be produced in various ways, some of which are,

- 1.) Radicals in solids
- 2.) Radiation damage centres
- 3.) Molecule-like complexes in a solid matrix
- 4.) Paramagnetic impurities

In our case, 4), the paramagnetic impurity is a copper dopant Cu^{2+} .

If we consider the case of a single paramagnetic ion which is not interacting with other impurity ions via dipole-dipole interactions and has a single unpaired electron in an S state with a "spin-only" magnetic dipole moment of $m_s g_s \beta$ ($m_s = 1/2$, β is the Bohr magneton, $g_s = g$ free electron), then in a magnetic field the spin degeneracy is resolved and the dipole may orient itself parallel or antiparallel to the external magnetic field with corresponding energies $\pm \frac{1}{2} g_s \beta H$, and this is the familiar Zeeman effect.

Considering an ensemble of such ions we may observe magnetic dipole transitions induced between these two levels by applying a high frequency magnetic field polarized perpendicularly to H which satisfies the resonance condition.

$$h\nu = g_s \beta H$$

Resonance absorption will then be observed corresponding to dipoles being shipped from parallel to antiparallel to \vec{H} .

Emission will also be induced although when the system remains in thermal equilibrium the population of $\vec{\mu}$ dipole parallel to H will exceed that of $\vec{\mu}$ dipole antiparallel to H , and a net absorption will occur.

Zeeman separations at 10K are typically 0.01cm^{-1} and $KT_{\text{room}} \sim 200\text{cm}^{-1}$ and since it is the slight difference in populations which gives rise to observable transitions the absorption is enhanced at lower temperatures. Another advantage of lower temperatures is that a major source of E.P.R. line broadening is spin-lattice relaxation and since spin-lattice relaxation time generally increases at lower temperatures the line width is reduced.

Other effects which cause line broadening are spin-spin interactions and exchange effects, neither of which are important in our case.

The spectra discussed here were all recorded at liquid nitrogen temperature (77°K).

Consider an ion having an orbitally non degenerate ground state with spin S . The "spin-only" interaction with an external magnetic field will be

$$= 2\beta\vec{H}\cdot\vec{S}$$

If \vec{H} is parallel to \vec{Z} then the term splits into $(2S+1)$ equally spaced levels with energies $2\beta H M_S$ and a separation $2\beta H$ between adjacent levels.

Magnetic dipole transitions will have intensities proportional to

$$P_{\epsilon} = |\langle \phi_{\text{Final}} | (L_{\epsilon} + g_S S_{\epsilon}) | \phi_{\text{Initial}} \rangle|^2$$

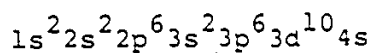
as a consequence of Fermi's Golden Rule. The subscript ϵ denotes the component along the direction of the magnetic vector of the incident radiation. With p_{ϵ} as above we have, ($\vec{H} = H\vec{z}$)

$$P_x = P_y = S(S+1) - M_S(M_S+1)$$

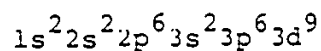
for the transition $|SM_S\rangle \rightarrow |SM_{S+1}\rangle$ and $P_x = P_y = P_z = 0$ for all other transitions. So we have the selection rule $\Delta M_S = \pm 1$. In practice this simple scheme is complicated by crystal field effects, spin-orbit coupling and hyperfine interactions. Hyperfine interaction between the electron and the magnetic moment of the nucleus results in a further splitting of each M_S level into $(2I+1)$ levels.

B. The divalent Copper Ion

The ground state of the copper atom has the electronic configuration



Thus giving a 2S term, the divalent copper ion has a configuration



Resulting in a 2D term, $L=2$, $s=1/2$. This can conveniently be treated as a hole in a closed 3d shell in the complementary scheme.

C. The Complete Hamiltonian

The complete hamiltonian operator for a paramagnetic ion in a crystalline field and zero magnetic field is

$$= T + V_c + V_{so} + V_x + V_{ss} + V_{sI} + V_Q \quad (III.1)$$

where;

$$T = \sum_k (p_k^2 / 2M)$$

is the total KE of the k^{th} electron with momentum p_k and mass M and the sum extends over all the electrons for the ion.

The Coulomb term V_c consists of

$$V_c = -\sum_k \frac{Ze^2}{r_k} + \frac{1}{2} \sum_{\substack{ij \\ i \neq j}} \frac{e^2}{r_{ij}}$$

The first term is the Coulomb attraction between the k^{th} electron and the nucleus and the second term is the Coulomb interaction between electrons summed over all electrons in the ion. The factor of 1/2 eliminates double counting.

The V_{so} term is the contribution due to spin-orbit coupling and can be written as

$$V_{so} = \sum_{ij} \lambda_{ij} \vec{l}_i \cdot \vec{s}_j$$

Where i and j are summed over all electrons in the ion.

With Russell-Saunders coupling this becomes

$$\sum_i \vec{l}_i = \vec{L} \text{ and } \sum_i \vec{s}_i = \vec{S}$$



And so V_{SO} becomes

$$V_{SO} = \lambda \vec{L} \cdot \vec{S}$$

where λ is the spin-orbit coupling constant and depends on some radial integral.

V_x represents the interaction between the paramagnetic ion and the crystal field potential

$$V_x = -\sum_k e \Phi(\vec{r}_k)$$

V_{SS} represents the magnetic dipole-dipole interaction between electrons and in our case can be set equal to zero since we are dealing with a dilute impurity with a single hole.

V_{SI} represents the magnetic interaction between unpaired electrons and the nuclear moments of both central ion and ligands. In our case no superhyperfine interaction was observed.

A full relativistic treatment of the interaction between an electron and the nuclear magnetic moment of the nucleus (see Griffith § 5.5.3) shows that the interaction adds a term

$$= 2\gamma\beta_N \vec{I} \cdot \left\{ f(r^{-3} \vec{I} - r^{-3} \vec{S} + 3r^{-5} (\vec{S} \cdot \vec{r}) \vec{r}) \right. \\ \left. + r^{-2} \frac{df}{dr} (\vec{S} - r^{-2} (\vec{S} \cdot \vec{r}) \vec{r}) \right\}$$

where $f = 1 - \frac{E + eA_0}{2mc^2}$ and is close to unity.

After a lot of heavy algebra and with the use of the replacement theorem of equivalent operators this can be written as (within a term):

$$H_m = P \left\{ \vec{L} \cdot \vec{I} - \kappa (\vec{S} \cdot \vec{I}) + \xi \left[L(L+1) \vec{S} \cdot \vec{I} - \frac{3}{2} (\vec{L} \cdot \vec{S}) (\vec{L} \cdot \vec{I}) - \frac{3}{2} (\vec{L} \cdot \vec{I}) (\vec{L} \cdot \vec{S}) \right] \right\}$$

with,

$$P = 2\beta_N \langle r^{-3} \rangle$$

γ depends on the nucleus in question and β_N is the nuclear magneton,

and,

$$\xi = \frac{2 + 1 - 4S}{S(2I-1)(2I+3)(2L-1)}$$

Within a d^n configuration there should not be a Fermi contribution of the form $\vec{S} \cdot \vec{I}$ but configuration interaction means that there is always an unpaired spin density at the nucleus from s wave contributions which are mixed in by configuration interaction. This warrants the term $K(\vec{S} \cdot \vec{I})$ but unfortunately there is no accurate way of calculating K .

V_Q represents the quadrupole interaction between the nuclear and electronic quadrupole moments and can be written as the equivalent operator:

$$\vec{I} \cdot \mathcal{Q} \cdot \vec{I}$$

Since in practice this is a small contribution, only diagonal elements are considered and application of $\vec{\nabla} \cdot \vec{E} = \rho$ gives the extra condition that $\text{Tr}(\mathcal{Q}) = 0$. If only $\Delta_{MI} = 0$ transitions are considered then $\text{Tr}(\mathcal{Q})$ is in any case indeterminate since it only adds a constant $\frac{1}{3}\text{Tr}(\mathcal{Q})I(I+1)$ to the Hamiltonian.

D. The spin Hamiltonian

The complete Hamiltonian as written in III.1 is too cumbersome to work with and in our case V_x is unknown.

For the fitting of the recorded spectra we make use of an equivalent Hamiltonian of the form:

$$H = \tilde{S} \cdot g \cdot \vec{H} + \tilde{S} \cdot A \cdot \vec{I} + \vec{I} \cdot Q \cdot \vec{I}$$

The first term is the electronic Zeeman term and the g "tensor" reflects anisotropy in the spectrum due to spin-orbit and crystal field effects. The \tilde{S} here is not the actual spin of the system but is an effective spin, often called "fictitious spin". $(2S+1)$ is equal to the number of electronic levels in the ground state of the ion.

The second term describes the magnetic hyperfine interaction discussed earlier. The A "tensor" describes both the magnetic interaction and the Fermi contact interaction.

The third term is an equivalent operator form for the interaction between the electronic and nuclear quadrupole moments as discussed earlier. The restriction $\text{Tr}(Q) = 0$ reduces the number of empirical factors needed to fit the spectrum since $\text{Tr}(Q)$ only adds a constant $\frac{1}{3}\text{Tr}(Q)I(I+1)$ to H if $\Delta_{MI} = 0$ only transitions are considered. It's inclusion is warranted by the fact that at certain orientations $\Delta_{MI} = \pm 1$ "forbidden" transitions are easily seen. This is because this non linear term in I means M_I is no longer a good quantum number.

If we choose a frame of reference which diagonalizes the g "tensor" then the Zeeman term can be written as

$$H = (S_x, S_y, S_z) \cdot \begin{pmatrix} g_x & 0 & 0 \\ 0 & g_y & 0 \\ 0 & 0 & g_z \end{pmatrix} \cdot \begin{pmatrix} H_x \\ H_y \\ H_z \end{pmatrix}$$

$$= (g_x S_x H_x + g_y S_y H_y + g_z S_z H_z)$$

Similarly for the A "tensor"

$$H = (A_x S_x I_x + A_y S_y I_y + A_z S_z I_z)$$

Although for low symmetries it may not be possible to diagonalize g and A simultaneously as we shall see.

CHAPTER IV
INSTRUMENTATION

A. K-Band Spectrometer

The K-band spectrometer used was of balanced bridge design, using a circulator, with the microwave frequency stabilized against the sample cavity. A block diagram is shown in fig. IV.1. The microwave power was supplied by a Varian model VA98E reflex klystron producing 30mW of power.

(1) Klystron Stabilizer

The klystron frequency was stabilized to the cavity resonant frequency using a Teltronic model KSLP Klystron Stabilizer. The stabilizer works on the principle of automatic frequency control (A.F.C.). A sine wave modulation of approximately 70 KHz was impressed on the reflector voltage thus causing a small amount of frequency modulation. If the Klystron frequency is tuned at or near the cavity resonant frequency, the output detected by the A.F.C. signal is amplified and then applied to the phase sensitive detector (P.S.D.) built into the stabilizer, which compares the signal with the original modulation signal. The result is a D.C. error voltage with a polarity and magnitude proportional to the difference between the klystron oscillator frequency and the resonant frequency of the cavity. The error voltage is applied to the reflector of klystron in such a manner that the klystron frequency is pulled back to the frequency

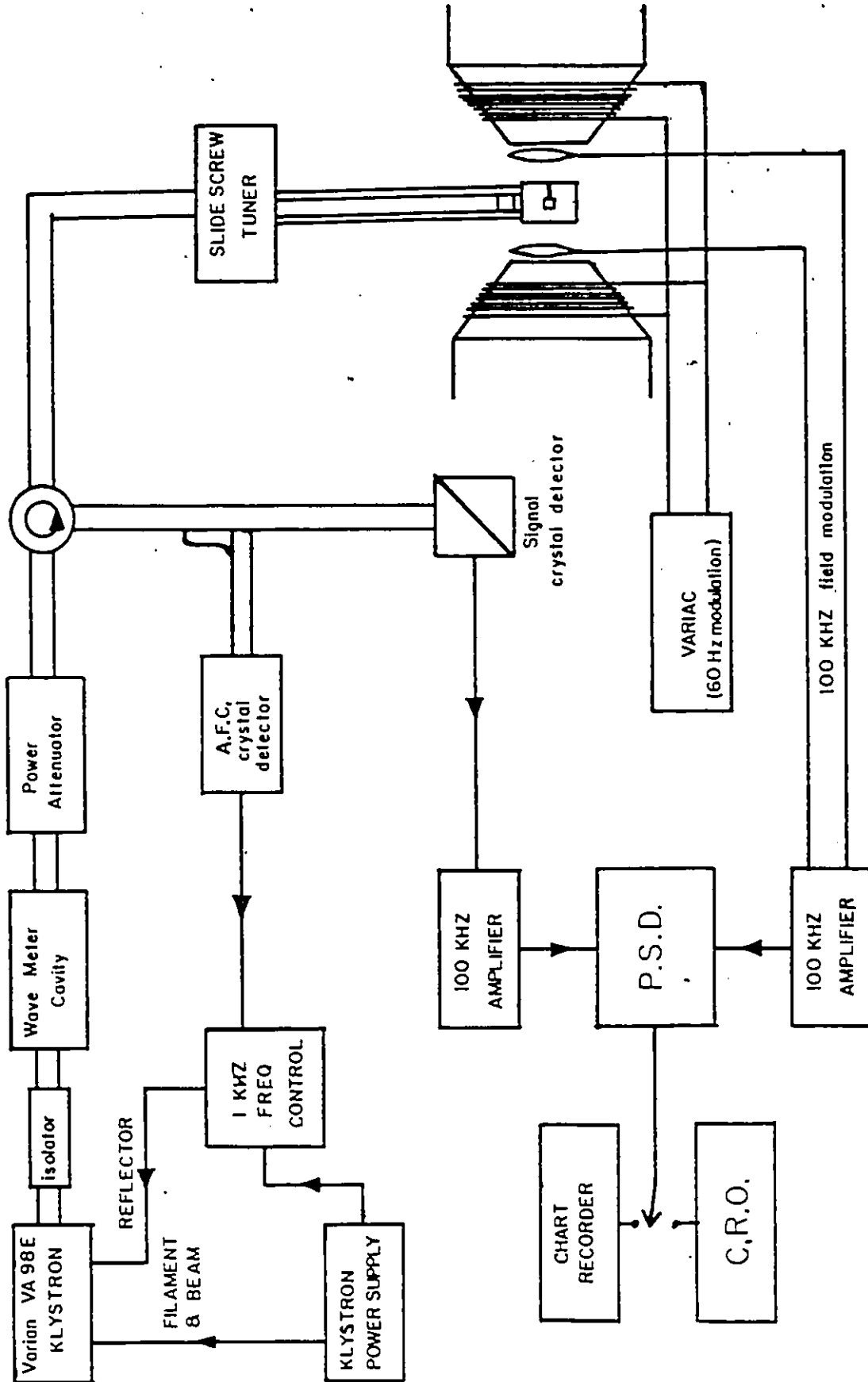


FIG IV. 1

of the cavity; thus stabilizing the klystron on the resonant frequency of the cavity.

(2) Microwave Circuit

Microwaves are prevented from re-entering the klystron by use of an isolator, which is a two terminal pair microwave ferrite device which makes use of the Faraday effect to permit transmission of microwaves in one direction and prevents their transmission in another direction. A tuneable cylindrical cavity is used as a wavemeter, and an attenuator is used to control the power reaching the sample cavity which may be necessary in cases of saturation.

A three port circulator is used to allow transmission of klystron power to the cavity and power reflected at resonance from the cavity to the detector, without power going directly to the detector or any reflected power returning to the klystron arm. The cavity arm can be matched to the klystron arm by means of a slide-screw tuner. Any E.P.R. absorption in the cavity then causes a mismatch, so that power is reflected from the cavity into the detector arm. In practice the cavity is slightly mismatched in order to allow sufficient power to bias the detector crystal.

Fig. IV.3 shows a diagram of the position of the diodes D_1 and D_2 in the detector waveguide and the transformer circuit. The lines show the distribution of E intensity and it can be seen that E_1 and E_2 are in antiphase so that the signals from

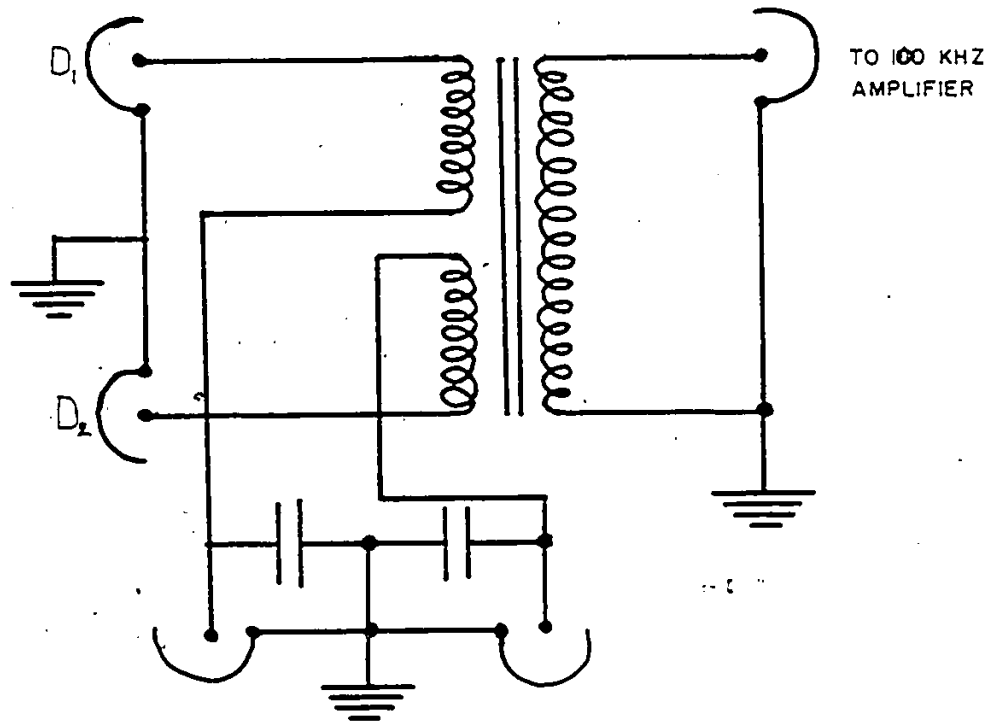
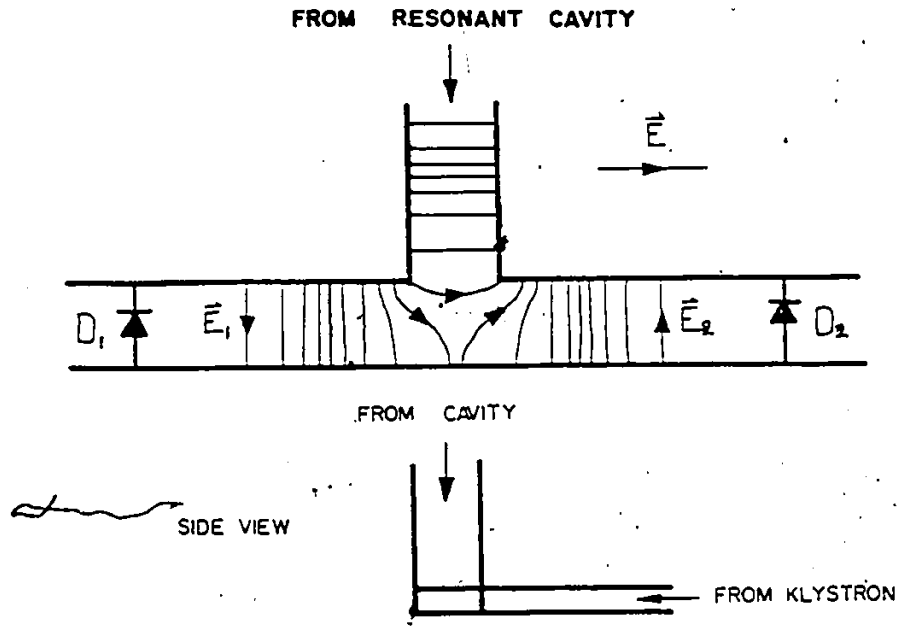


FIG IV.3

D_1 and D_2 are also in antiphase. D_1 and D_2 transmit the signal to the 100 KHz amplifier through a transformer with two oppositely directed windings and since noise at D_1 and D_2 is random it will tend to cancel half the time, thus resulting in reduced noise.

The resonant signal is preamplified and then fed into the Princeton Applied Research (P.A.R.) model J.B.-6 lock-in Amplifier, which compare the phase and frequency of the resonant signal with the original 100 KHz modulation signal in the same manner as the P.S.D. of the A.F.C. circuit. The result is a derivative signal proportional to the resonant signal, which can be displayed on the oscilloscope or chart recorder as a function of magnetic field. To facilitate display on the oscilloscope the magnetic field is modulated at 60 Hz with a "Variac", in addition to the 100 KHz modulation. The horizontal sweep of the oscilloscope is connected to a 60 Hz source and synchronised with the modulation using a phase shifter. The method of oscilloscope display allows one to observe E.P.R. signals as both the magnetic field and crystal orientation are varied.

This provides a convenient and rapid means of studying angular variations.

The cylindrical cavity used was made of glass with an internal surface sputtered with gold. Operating in the TE₀₁₁ mode the cavity has been employed successfully in this laboratory on previous occasions. In conjunction with the cavity is a rotating mechanism previously developed in this laboratory⁶. It facilitates rotation about a horizontal axis which combined with rotation of the magnet about the vertical axis allows an arbitrary orientation of magnetic field.

(3) External Magnetic Field and Modulation

The external magnetic field is produced by a 12 inch Varian electromagnet with a 3.5 inch gap and a rotating base. The magnet is stabilized by a Fieldial model V-FR 2503 (Varian) control unit, which keeps the field value constant to within one Gauss for several hours. It is possible to achieve a linear sweep of up to 20 KGauss.

Magnetic field modulation at 100 KHz is generated by an oscillator built into the P.A.R. lock in amplifier. This signal is amplified externally and applied to two Helmholtz coils connected in series and mounted on either side of the cavity.

B. Proton Magnetometer

Measurements of magnetic field strength are obtained by means of a proton magnetic resonance oscillator, tuning circuit and amplifier, together with a wide band amplifier and electronic counter, Hewlett-Packard No. 5253. Several complementary probes using rubber as a proton source were constructed previously in this laboratory to cover a wide frequency range and one probe proved sufficient for all measurements.

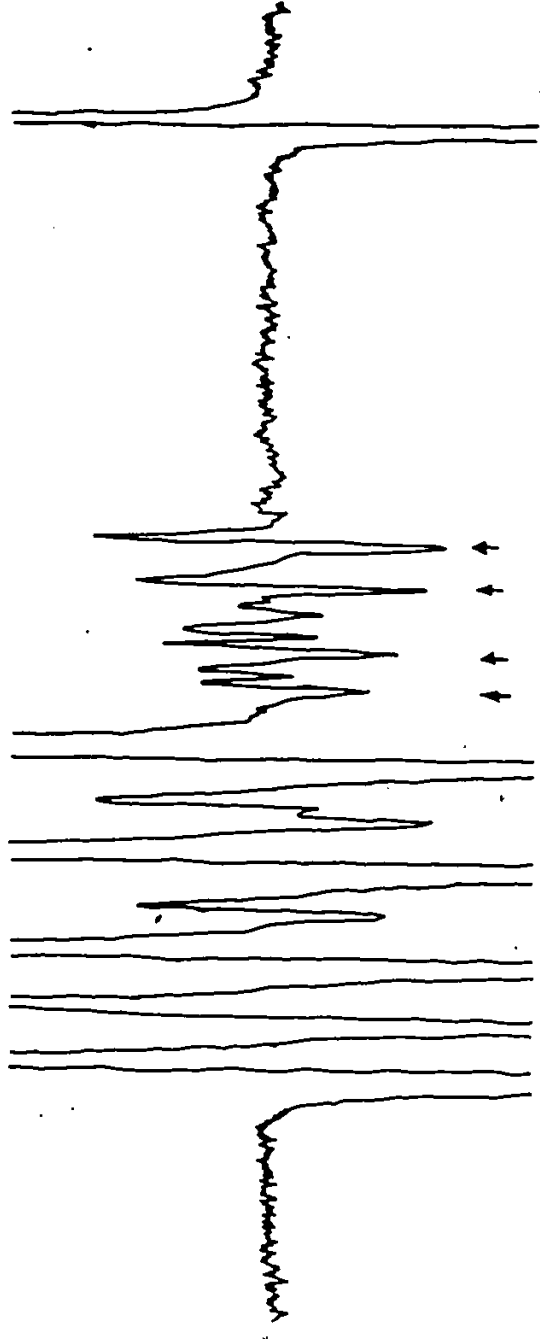
CHAPTER V
EXPERIMENTAL PROCEDURE

(1) Crystal Orientation

Because the crystals grow preferentially along the b-axis visual examination with the aid of a binocular microscope enabled mounting of the crystals within $\pm 5^\circ$. The crystals were attached to the quartz capillaries with epoxy resin and this facilitated placing a thermocouple (copper-constantan) in the capillary in good thermal contact with the crystal for studies of the temperature dependence of the spectra.

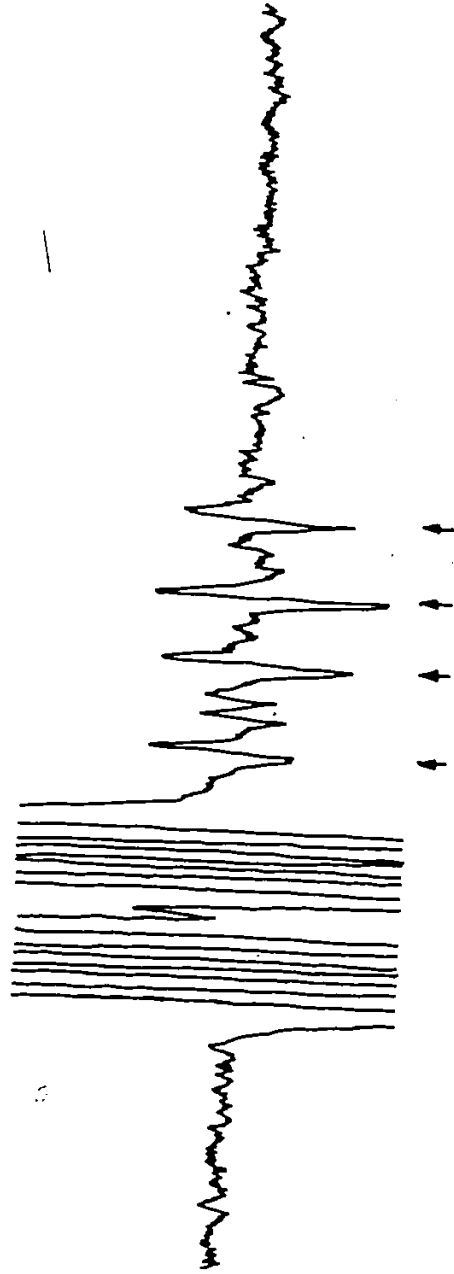
Using the orientation of the magnetic field about a vertical axis and the crystal about a horizontal axis with arbitrary zero the orientations of the magnetic field relative to the crystal were plotted on a stereogram. The accuracy of orientation was checked by recording spectra on a chart recorder at a point where the spectra coincided and then recording the spectra for the magnetic field in the reverse direction; for perfect alignment the spectra should have been identical, in practice deviations of less than $\pm 0.5^\circ$ were observed. Hence the size of the error bars in the following diagrams.

Diagrams of the spectra in the three crystallographic directions are shown in figs. IV.1-3.



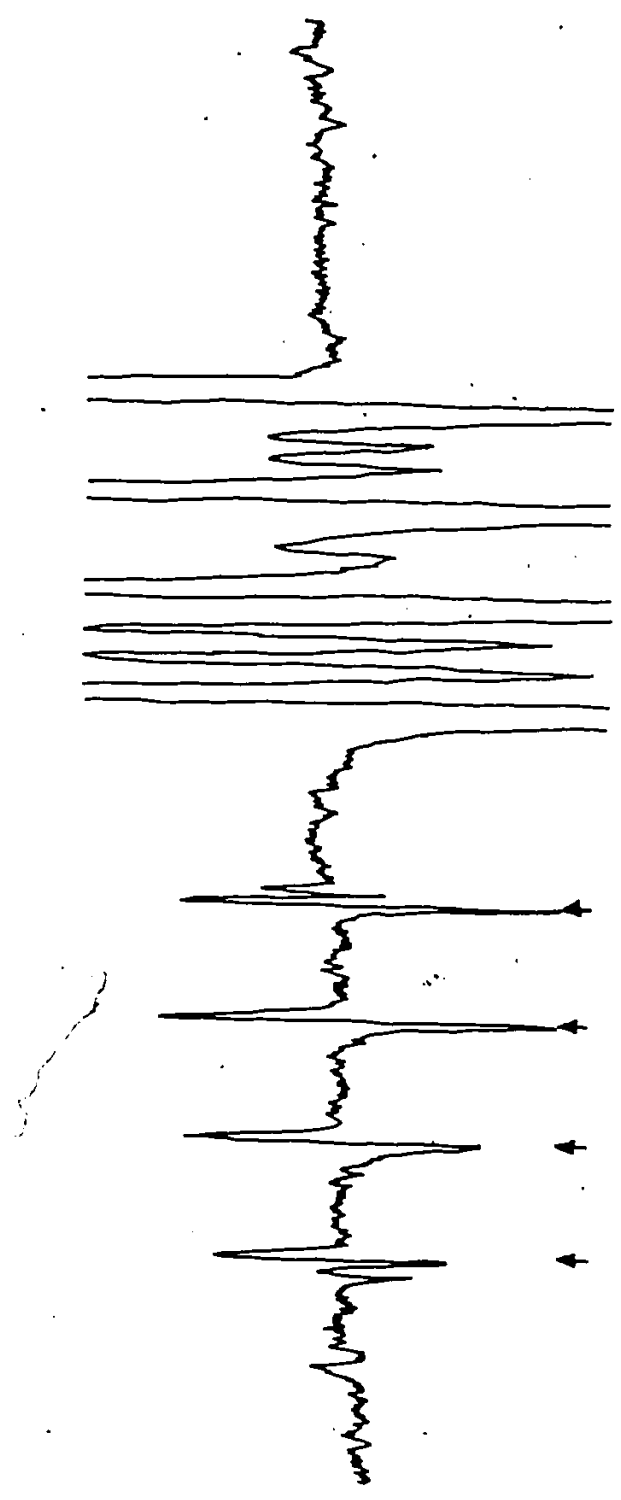
Magnetic field parallel to b

FIG IV.1



Magnetic field parallel to a

FIG IV.2



Magnetic field parallel to c

FIG IV. 3

The spectra displayed three mutually orthogonal axes coincident with the crystallographic axes at which the three sets of strong lines coincided to form a single set of four lines.

In the planes defined by these axes each set of four lines splits up into two sets of four lines consistent with the unit cell of $Z=4$ with four sets of crystallographically inequivalent centres for an arbitrary orientation of magnetic field.

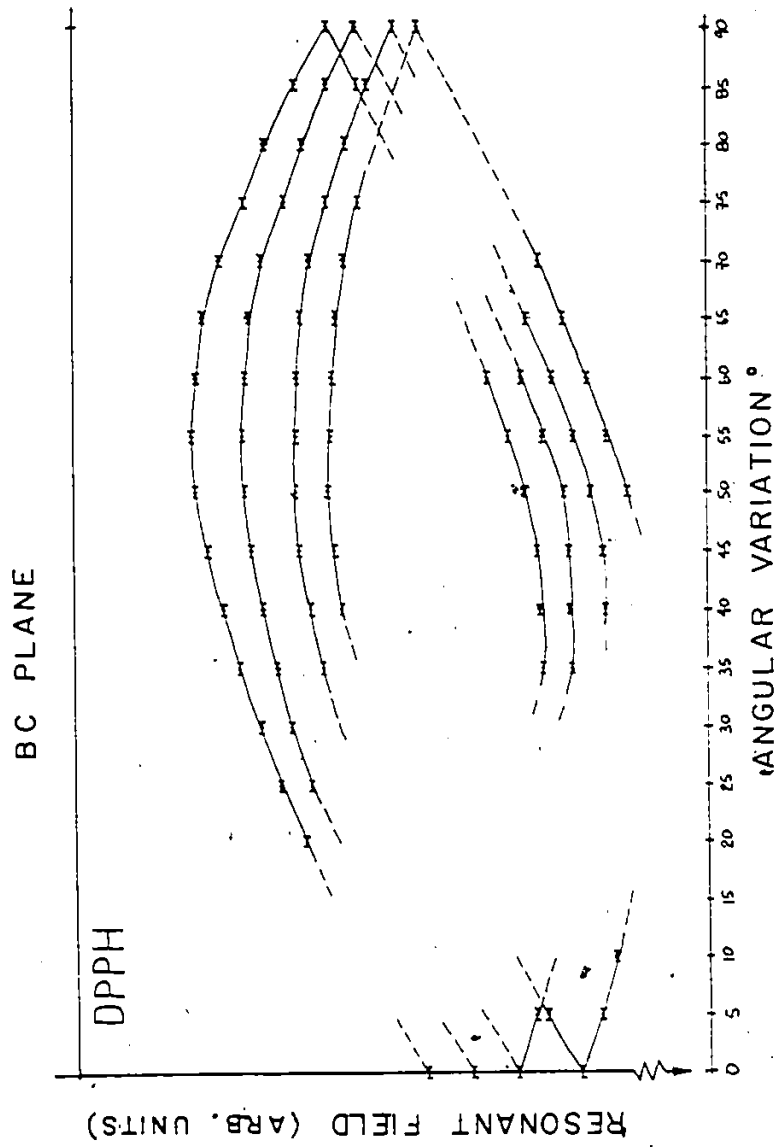
The angular variation of the set of weak lines is shown in figs. IV 4-6 in the ab , bc , ca planes, the gaps occur where the variation was obscured by the set of strong lines.

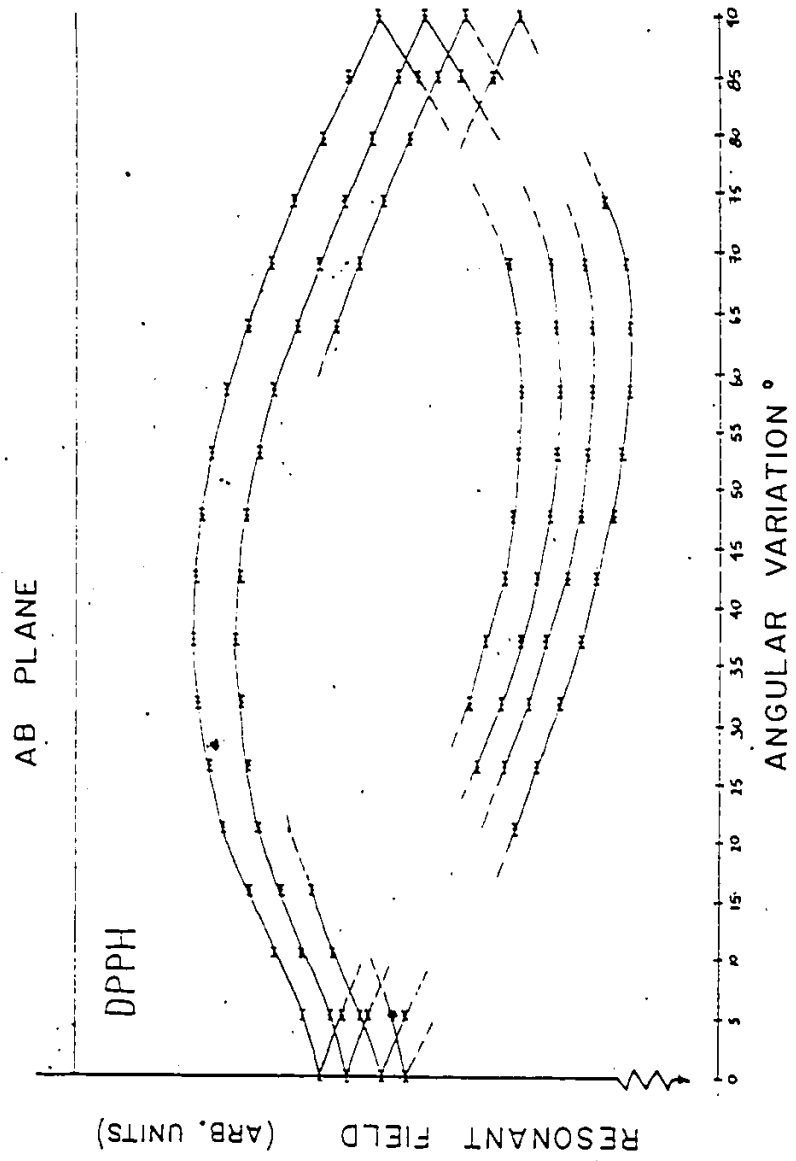
The orientation of the crystallographic axes was confirmed by x-ray analysis (see appendix 2).

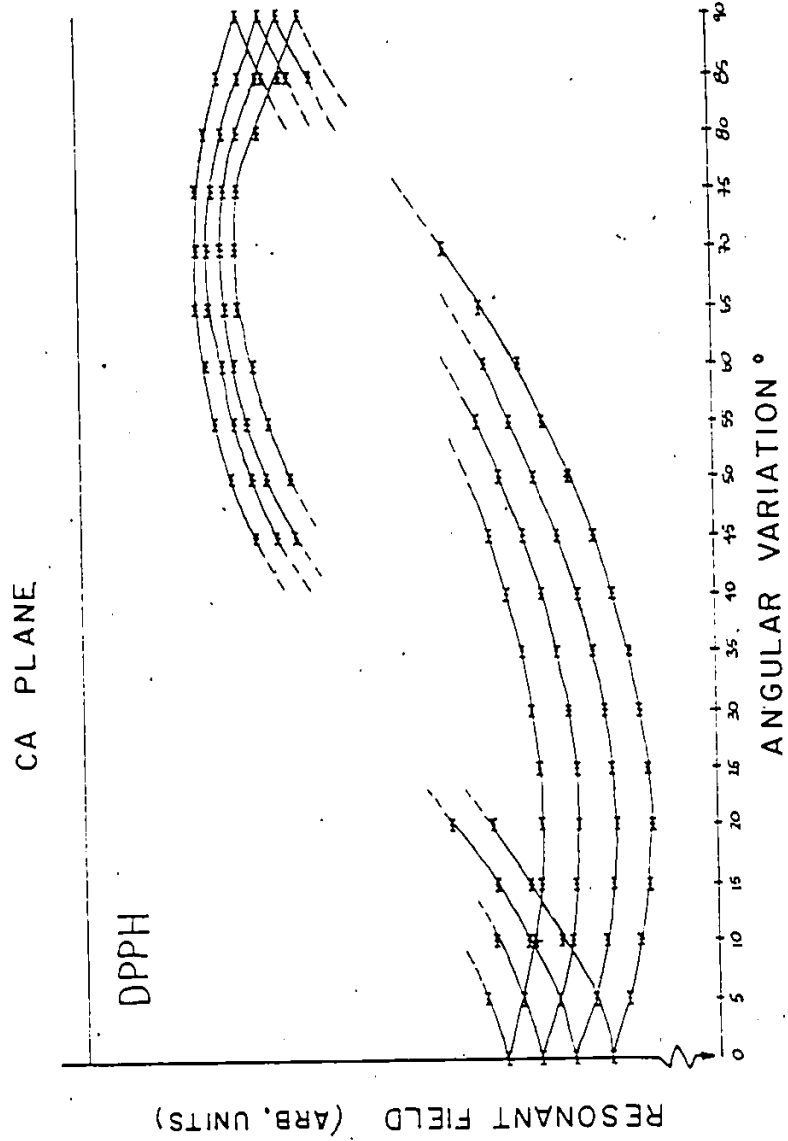
Measurements were taken with a crystal doped with a single isotope Cu^{63} and measurements of resonant fields were recorded for 38 orientations, and the directions of magnetic field for a right-handed system of co-ordinates were calculated directly from a plot of all 38 orientations on a stereogram. This allowed for convenient elimination of systematic errors and corrections for misalignment mentioned earlier.

The measurements were taken at orientations a few degrees apart wherever all four lines were not obscured by the stronger ones.

For a batch of crystals grown with Cu^{63} ions, many crystals turned out to be twinned, resulting in a complicated addition of spectra and were of no use for this work.







To check that the spectra were in fact due to twinning one crystal was removed from the spectrometer and carefully sliced into two and one half discarded. The spectrum resulting from half the original crystal showed a change of relative intensity of the extra lines with respect to the known set thus confirming their origin as a twinned region of crystal.

The results are tabulated in appendix I.

(3) Measurement of Magnetic Field

A set of probes covering the frequency range 30 MHz to 53 MHz had previously been constructed in this laboratory and a single probe proved sufficient for all of our measurements.

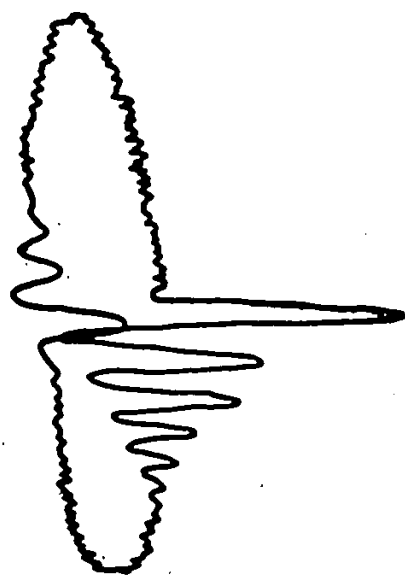
A satisfactory signal intensity was achieved by using a grounded brass tube shielding two stiff wires which carried current to the inductor and which were separated from each other and the shielding by spacers set at intervals along the tube (see fig. V.7).

Actual measurements were made using a double-beam oscilloscope. The crystal rotator and magnet scale were set at the required orientation. Each E.P.R. line in turn was centred on one of the oscilloscope beams, using the second beam the P.M.R. line was tuned to the E.P.R. line. The frequency of oscillation of the P.M.R. signal was then read from the digital output of the electronic counter. This can be converted to a magnetic field strength using the relation

$$h\nu = g_p \beta_N H$$

$$H = \frac{h}{g_p \beta_N} \cdot \nu$$

$$\text{or } H(\text{KGauss}) = 0.234869 \nu(\text{MHZ})$$



C.R.O. display of P.M.R. signal .

FIG V. 8

where;

H is magnetic field strength

h is Planck's constant

g_p is the proton g-value

β_N is the nuclear magneton

ν is the frequency of oscillation

Typical C.R.O. display is shown in fig V.8.

Since the 60 Hz modulation was only 20 Gauss the error in reading C.R.O. scale could not have exceeded 2 Gauss and was thus of no concern as a major source of error.

(4) Measurement of Microwave Frequency

A small amount of the free radical D.P.P.H. (diphenyl picryl hydrazyl) was attached to the sample with glycerine and acted as a marker to measure the microwave frequency using the relation

$$h\nu = g_{DPPH} H_{DPPH}$$

$$\nu = \frac{g_D \beta}{h} \cdot H_D$$

where;

ν = microwave frequency

g_D = D.P.P.H. g value = 2.0036

H_D = field value at D.P.P.H. resonance.

The D.P.P.H. E.P.R. line is extremely exchange narrowed and gives a very narrow temperature independent line.

CHAPTER VI

DEVELOPMENT OF COMPUTER PROGRAM FOR FITTING OF DATA

A. The method

A method of parameter fitting using multi-dimensional Newton-Raphson Least-Squares minimization developed by Dr. W. E. Baylis was used so that the program could be generalized. This enabled it to accept data at any orientation and to fit a curve using data from different orientations rather than different frequencies.

The one dimensional Newton-Raphson Method⁷ is obtained analytically from the following condition on the Taylor series expansion

$$f(\chi_n+h) = f(\chi_n) + h \cdot f'(\chi_n) + \frac{h^2}{2!} f''(\chi_n) + \dots = 0$$

Where χ_n is an approximation of the root of the equation. This can be written in partial derivative form as

$$\frac{\partial}{\partial \chi_n} f(\chi_n + h) = \frac{\partial}{\partial \chi_n} f(\chi_n) + h \cdot \frac{\partial}{\partial \chi_n} f'(\chi_n) + \dots = 0$$

The problem of fitting the experimental data can be overcome in the following way. The Hamiltonian can be expressed as a function of a number of fitting parameters p_i ($i = 1, 2, \dots, I_{\max}$), the experimentally measured magnetic field values B_1 and other experimental parameters necessary such as orientation K or temperature T . B is a function of orientation so that the resonant fields occur as $(N-1)$ values for each of M orientations.

where N will represent the degeneracy of the ground state. So the Hamiltonian can be expressed as

$$H = H(p_1, p_2, \dots, p_{I_{\max}}, \vec{B}, \hat{K}, T, \dots) \quad \text{VI.1}$$

The Hamiltonian is represented in an n -dimensional basis

The matrix elements for the Hamiltonian and its first and second derivatives with respect to the parameters must be known or able to be calculated.

$$\langle \alpha | H | \beta \rangle \quad \text{VI.2}$$

$$\langle \alpha | \partial H / \partial p_i | \beta \rangle \quad \text{VI.3}$$

$$\langle \alpha | \partial^2 H / \partial p_i \partial p_j | \beta \rangle \quad \text{VI.4}$$

The matrix elements of VI.2 and VI.3 for our Hamiltonian are easily calculated knowing the matrix elements of $I = 3/2$ and $S = 1/2$ within the manifold of $\{ |\tilde{S}\rangle \otimes |\tilde{I}\rangle \}$. As the parameters occur linearly in the Hamiltonian with no cross products the elements of VI.4 will be zero.

For each set of external parameters (B, K, T, \dots) , (in this case for $M(N-1)$ resonant field values), the Hamiltonian is diagonalized using the subroutine is basically an extension of the Jacobi method to Hermitean matrices^{8,9} and is double precision, complex.

A new set of basis vectors $\{ |i\rangle \}$, (in terms of the original set $\{ |\alpha\rangle \}$, $|i\rangle = \sum_{\alpha} c_{\alpha} |\alpha\rangle$) is then obtained in which the Hamiltonian is diagonal

$$\langle i | H | j \rangle = E_i \delta_{ij} \quad \text{VI.5}$$

The difference between one adjacent pair of eigenenergies $(E_{k_1} - E_{k_2})$ will correspond to the transition energy experimentally

determined from measurement of the microwave frequency ν_k . The correspondence between the pair of eigenenergies chosen and the resonant field representing that transition must be known. In this case the correspondence was determined and the programming simplified by taking all measurements at orientations above the resonant lines were clearly observed.

A least squares sum is formed from:

$$f = \{(E_{k_1} - E_{k_2}) - \nu_k\}^2 \quad \text{VI.6}$$

$$= \{(E_{k_1} - E_{k_2}) - \frac{g_D H_D}{g_s}\}^2 \quad \text{VI.7}$$

where the transition energy in VI.7 is expressed in units of Gauss and is determined from the resonant field of DPPH (H_D). The value of the least squares sum f is then determined by summing over the total number of transitions measured $(N-1)M$ and dividing by the number of degrees of freedom $(N \text{ free} = \text{number of transitions} - \text{number of parameters})$.

The multi dimensional Newton-Raphson method finds the value of $P = (p_1, p_2, \dots, p_i)$, representing a vector in i -dimensional space where i is the number of parameters, such that $\frac{\partial f}{\partial p_i}(P) = 0$ by solving iteratively the equation for the displacement :

$$\frac{\partial f(P + \delta)}{\partial p_i} \approx \frac{\partial f(P)}{\partial p_i} + \sum_j \frac{\partial^2 f(P)}{\partial p_i \partial p_j} \delta_j = 0$$

the solution is:

$$\delta_i = -\sum_j M_{ij} \frac{\partial f(P)}{\partial p_j} \quad \text{VI.8}$$

where (M_{ij}) is the inverse of $(\frac{\partial^2 f(P)}{\partial p_i \partial p_j})$

and

$$\sum_j M_{ij} \frac{\partial^2}{\partial p_j \partial p_i} f(p) = \delta_{ii}$$

The inversion is carried out by the subroutine DMINV (see appendix 5). The value of S_i is then added to p_i to give the new estimate of the parameter.

The first and second derivatives of the least squares sum f required in the calculation are determined using perturbation theory.

$$\begin{aligned} \frac{\partial f}{\partial p_i} &= \frac{\partial}{\partial p_i} \frac{\sum_k \left\{ (E_{k_1} - E_{k_2}) - \frac{g_D H_D}{g_s} \right\}^2}{N_{\text{free}}} \\ &= 2 \sum_k \left(\frac{\partial E_{k_1}}{\partial p_i} - \frac{\partial E_{k_2}}{\partial p_i} \right) \frac{\left\{ (E_{k_1} - E_{k_2}) - \frac{g_D H_D}{g_s} \right\}}{N_{\text{free}}} \end{aligned} \quad \text{VI.9}$$

and

$$\begin{aligned} \frac{\partial^2 f}{\partial p_i \partial p_j} &= 2 \sum_k \left\{ \left(\frac{\partial E_{k_1}}{\partial p_i} - \frac{\partial E_{k_2}}{\partial p_i} \right) \left(\frac{\partial E_{k_1}}{\partial p_j} - \frac{\partial E_{k_2}}{\partial p_j} \right) \right. \\ &\quad \left. - \left(\frac{\partial^2 E_{k_1}}{\partial p_i \partial p_j} - \frac{\partial^2 E_{k_2}}{\partial p_i \partial p_j} \right) \frac{\left\{ (E_{k_1} - E_{k_2}) - \frac{g_D H_D}{g_s} \right\}}{N_{\text{free}}} \right\} \end{aligned} \quad \text{VI.10}$$

where

$$\frac{\partial E_k}{\partial p_i} = \lim_{\delta_i \rightarrow 0} \left\{ \frac{E_k(p + \delta_i \hat{i}) - E_k(p)}{\delta_i} \right\}$$

Where \hat{i} is a unit vector in i -dimensional parameter space and where $E_k(p + \delta_i \hat{i})$ is the eigenenergy corresponding to $E_k(p)$ of the Hamiltonian $H(p + \delta_i \hat{i})$, to first order in δ_i

$$H(p + \delta_i \hat{i}) \approx H(p) + \frac{\partial H(p)}{\partial p_i} \delta_i$$

Using perturbation theory the eigenenergy can also be expressed to first order in δ_i

$$E_k(\underline{p} + \delta_i \hat{i}) = E_k(\underline{p}) + \langle k | \frac{\partial H}{\partial p_i} | k \rangle \delta_i$$

and consequently

$$\frac{\partial E_k}{\partial p_i} = \langle k | \frac{\partial H}{\partial p_i} | k \rangle \quad \text{IV.11}$$

similarly

$$\frac{\partial^2 E}{\partial p_i \partial p_j} = \lim_{\delta_i \delta_j \rightarrow 0} \frac{E(\underline{p} + \delta_i \hat{i} + \delta_j \hat{j}) - E(\underline{p} + \delta_i \hat{i}) - E(\underline{p} + \delta_j \hat{j}) + E(\underline{p})}{\delta_i \delta_j}$$

Now to second order in δ 's

$$\begin{aligned} H(\underline{p} + \delta_i \hat{i} + \delta_j \hat{j}) &= H(\underline{p}) + \frac{\partial H}{\partial p_i} \delta_i + \frac{\partial^2 H}{\partial p_i \partial p_j} \delta_i \delta_j \\ &+ \frac{\partial H}{\partial p_j} \delta_j + \frac{1}{2} \left(\frac{\partial^2 H}{\partial p_i^2} \delta_i^2 + \frac{\partial^2 H}{\partial p_j^2} \delta_j^2 \right) \\ &= H(\underline{p}) + V \end{aligned}$$

where V may be considered a small perturbation. As the parameters appear linearly in the Hamiltonian the last item goes to zero. By second order perturbation, the eigenenergies are shifted to

$$E(\underline{p} + \delta_i \hat{i} + \delta_j \hat{j}) = E(\underline{p}) + \langle k | V | k \rangle + \sum_{l \neq k} \frac{\langle k | V | l \rangle \langle l | V | k \rangle}{E_k - E_l}$$

Thus

$$\frac{\partial^2 E}{\partial p_i \partial p_j} = \langle k | \frac{\partial^2 H}{\partial p_i \partial p_j} | k \rangle + 2 \operatorname{Re} \sum_{l \neq k} \frac{\langle k | \frac{\partial H}{\partial p_i} | l \rangle \langle l | \frac{\partial H}{\partial p_j} | k \rangle}{E_k - E_l}$$

where the matrix elements $\langle k | M | l \rangle$ written in terms of the old basis are

$$\langle k|M|l \rangle = \sum_{\alpha, \beta} \langle k|\alpha \rangle \langle \alpha|M|\beta \rangle \langle \beta|l \rangle \quad \text{VI.12}$$

The similarity transformation is carried out by the sub-routine STCM (see appendix 5)

Probable errors are calculated as follows, since f may have a probable error given by $\Delta f \approx f/N_{\text{free}}$ the corresponding σ_i in p_i is given by

$$\Delta f \frac{1}{2} \sum_{ij} M_{ij} \sigma_i \sigma_j \approx f/N_{\text{free}}$$

The values of σ_i^2 are calculated from inversion of the above giving,

$$\sigma_i^2 = 2M_{ii}^{-1} (f/N_{\text{free}})$$

B. The flow chart

From the flow chart (see fig. VI.1) the steps in the computational process can be followed.

1. The data is read in including all external parameters, initial estimates of the crystal parameters and the matrix elements of operators required in the equivalent Hamiltonian. The input data after conversion is printed out.
2. The matrix elements that are independent of the field are calculated.
3. The remaining field dependent matrix elements are calculated using the components of the measured field values in addition to data utilised in 2. (see appendix 6 for RTN1)

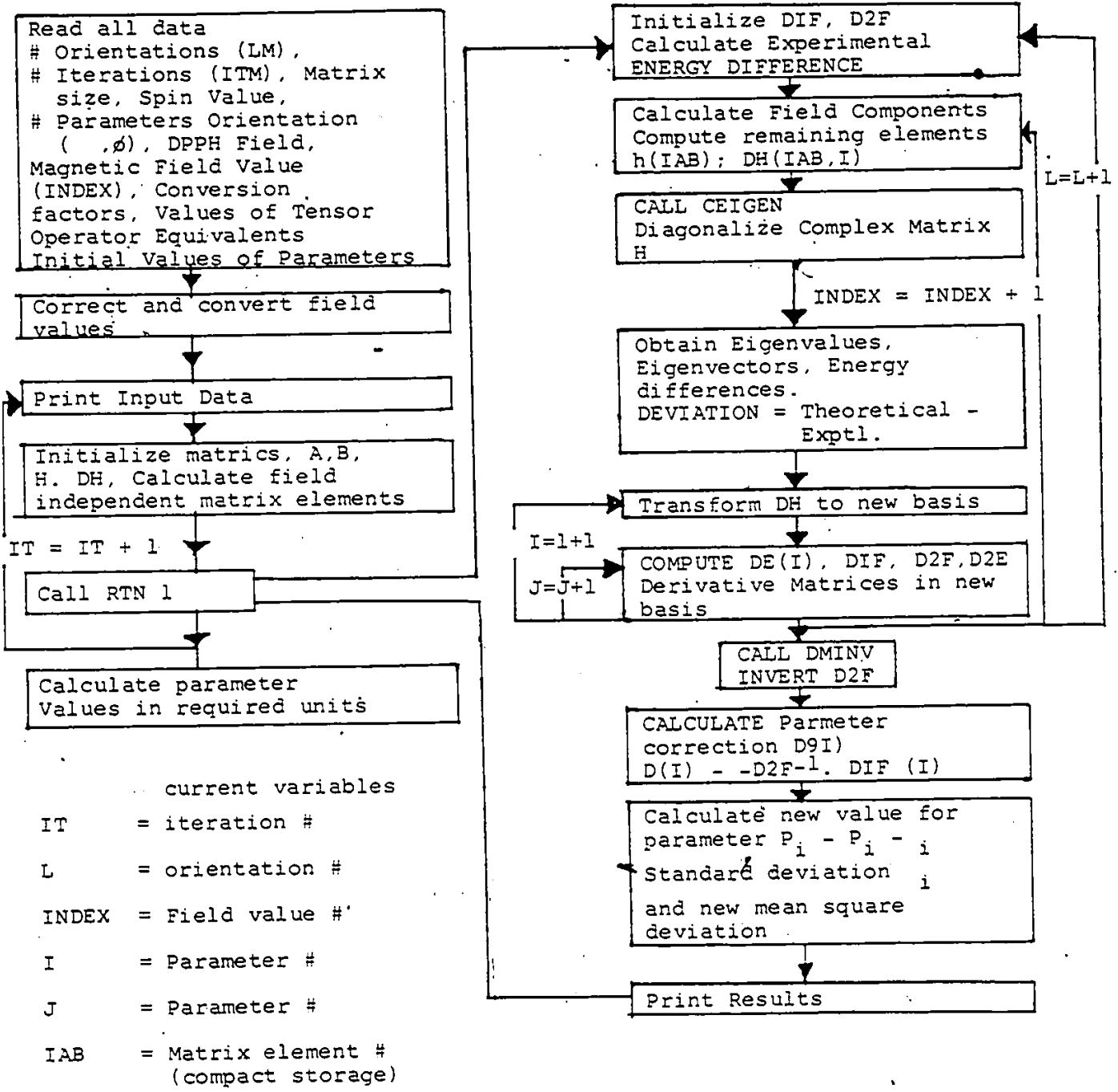


Fig. VI.1. FLOW CHART FOR COMPUTER PROGRAMME

4. The Hamiltonian matrix form in 2 and 3 is then diagonalized exactly using the subroutine CEIGEN (see appendix 7) which returns eigenenergies and eigenvectors. The difference between the adjacent eigenvalues provides the basis of the least squares sum while the eigenvectors are used in the similarity transformation in the next step. The value of DEVIATION printed out is a measure of the fit.
5. The derivative matrix is then transformed to the new basis in which the Hamiltonian is diagonal, see (VI.12). This then allows calculation of DE(I), the derivative of the energy with respect to each parameter, see (VI.11). From these the first and second derivatives of the least squares fit are formed, D1F(I), see VI.9, and D2F(I), see VI.10.

Step 5 is repeated for each parameter in the $I = I + 1$ loop, while the computation of the second derivative is repeated for all parameters J, with each parameter I in the $J = J + 1$ loop.

Steps 3 - 5 are then repeated for each of the $(N - 1)$ resonant fields at a given orientation during the INDEX = INDEX + 1 loop, which itself is repeated for all of the orientations in the $L = L + 1$ loop.
6. As D2F involves summation of both I & J simultaneously as well as a summation over all of the resonant fields, it is not completed until the end of step 5. D2F is then inverted using DMINV (see appendix 7). The parameter connection D(I) can then be calculated see VI.8,

the new estimate of the parameters is then determined

$$P(I) = P(I) + D(I)$$

The standard deviation for each parameter is then calculated together with an estimate of what the mean square deviation will be, using the new parameter values.

7. The results are printed and control returned to the main program where steps 2 to 7 are repeated for the number of iterations specified.
8. The parameters are converted to whatever units are required and any auxiliary calculations with the parameters may also be carried out here.

As a check on the inversion process and the reliability of the parameter values, the $D2F$ and $(D2F)^7$ matrices are multiplied using the subroutine DGMPRO (see appendix 8), based on IBM routine GMPROD)¹⁰ to see that the product is the unit matrix. (see VI.8)

C. Rate of Convergence

To indicate the rate of convergence a sample run is shown in table VI.1 giving the mean square deviation in KGauss.

TABLE VI.1

Iteration Number	Mean Square Deviation (KGauss) ²
1	0.9190
2	0.0220
3	0.0550
4	0.0022
5	0.0200
6	0.0006

Even though the values oscillates it can be seen that convergence is quite rapid.

CHAPTER VII

DISCUSSION AND CONCLUSION

In total thirty eight orientations were used to collect data; with orientations in all three planes included. For the fitting of parameters in the spin Hamiltonian nineteen were rejected because they gave for larger deviations from the trial energy levels than the remaining twenty nine. In excess of a dozen iterations were needed before an acceptable fit was obtained and from then on the quality deteriorated.

The best fit parameters are tabulated in table VII.1. The results are presented in the co-ordinate system discussed previously.

These results will be discussed in the light of previous reports, Abdulsabirov¹ had investigated the three strong sets of lines and had fitted data to an orthothombic spin Hamiltonian,

$$H = \vec{H} \cdot \vec{g} \cdot \vec{S} + \vec{S} \cdot \vec{A} \cdot \vec{I}$$

in which the g and A "tensor" shared common principal axes. They found that the orientations of these three sets axes were completely different and correlated these orientations with the crystallography with the help of X-ray analysis.

TABLE VII.1

g values

g _{xx}	g _{yy}	g _{zz}
2.5396 ± .0001	2.1296 ± .0002	2.0920 ± .0001
g _{xy}	g _{zx}	g _{zy}
0.1023 ± .0001	0.0347 ± .0001	0.0516 ± .0002

A values (x10⁻⁴ cm⁻¹)

A _{xx}	A _{yy}	A _{zz}
205.3 ± 0.9	19.9 ± 5.6	38.5 ± 4.0
A _{xy}	A _{zx}	A _{zy}
88.3 ± 2.0	2.3 ± 1.6	-36.9 ± 4.5

Q values (x10⁻⁴ cm⁻¹)

Q _x	Q _y
20.6 ± 2.0	3.8 ± 0.6

N.B.: Above expressed in crystallographic coordinate system described earlier.

Since Cu²⁺ is doubly charged, it substitutes for K¹⁺ in the lattice of K₂SO₄ overall electrical neutrality can only be preserved if some kind of charge compensation occurs. Abdulsabirov¹ proposed that this compensation occurs via a vacancy on an adjacent K¹⁺ site. A diagram of the crystal structure of K₂SO₄ projected along the c-axis is shown in fig. VII.1. The K₁ and K₂ sites differ in environment but the four of which occur in each

unit cell are related by the symmetry of the crystal. If the Cu^{2+} impurity substitutes for a K^{1+} as proposed by Abdulsabirov¹ then a vacancy on an adjacent K^{1+} site will strongly influence the g tensor and will rotate on principal axis towards the direction joining the Cu^{2+} impurity and the vacancy. Abdulsabirov¹ found that the above is consistent with Cu^{2+} substituting for K^{1+} on a K_2 type site with a vacancy on an adjacent K_1 type site. They found that the principal axis of the g tensor (ie. largest principal value) for the three centre types was within a few degrees of the line joining the K_1 and K_2 type positions. These $\text{K}_2^+ - \text{K}_1^+$ directions are marked 1,2,3 on fig. VII.1. They also mention the fourth weak set of lines investigated here and suggest that they may be due to a centre produced when charge compensation occurs on the fourth adjacent K_1^+ site. The line joining K_2^+ to this fourth adjacent site drawn and labelled 4 in fig. VII.1. The directions of the principal values of the g tensor observed by Abdulsabirov¹ are inconsistent with Cu^{2+} substituting on a K_1 type site and charge compensation occurring on a K_2 type site as can easily be verified. Why substitution should occur on K_2 and not K_1 type sites is not known but it can be noted that K_1 type sites have an oxygen much closer than K_2 type sites.

Our results are in fair agreement with the above as follows. The fitted parameters in table VII.1 indicate that the g "tensor" can be adequately fitted by a symmetric tensor and the A "tensor" not so adequately although as can be seen any observed asymmetry in A is slight.

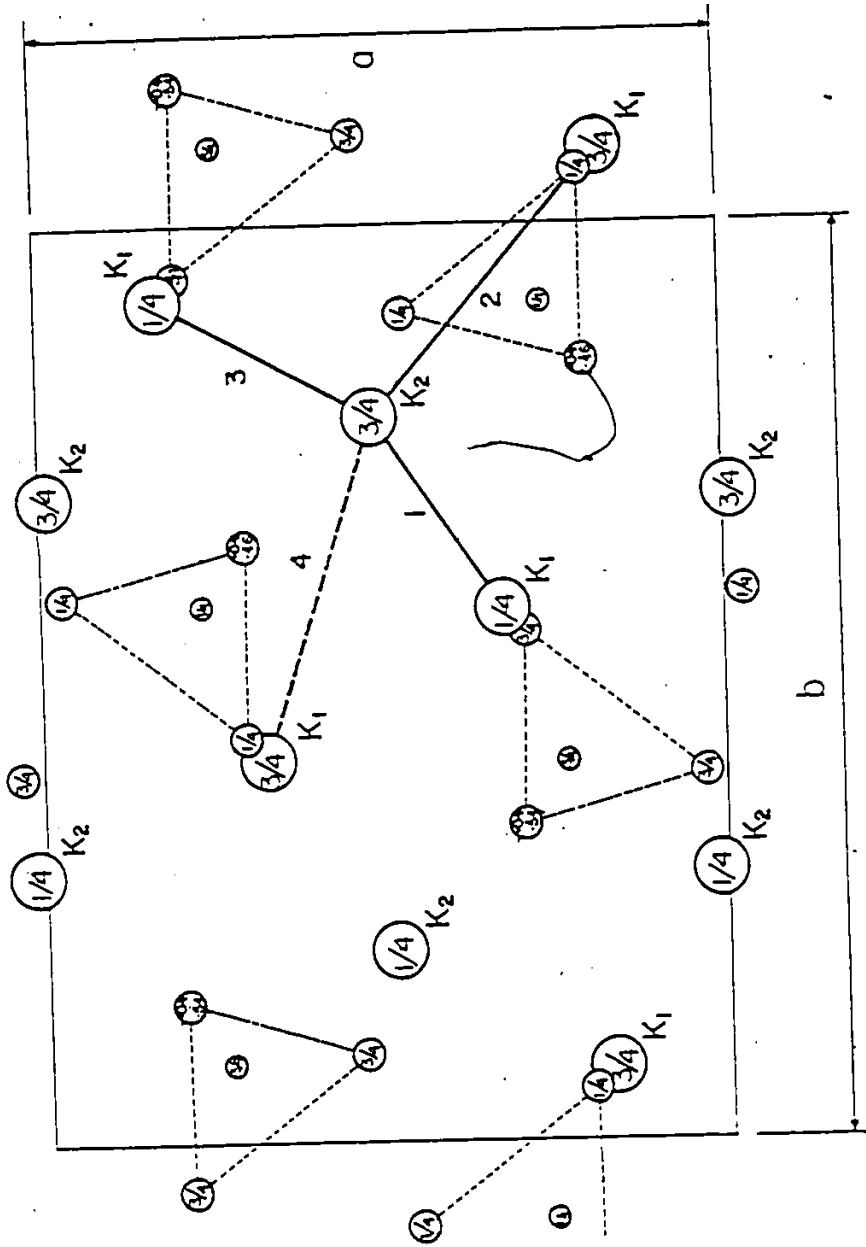
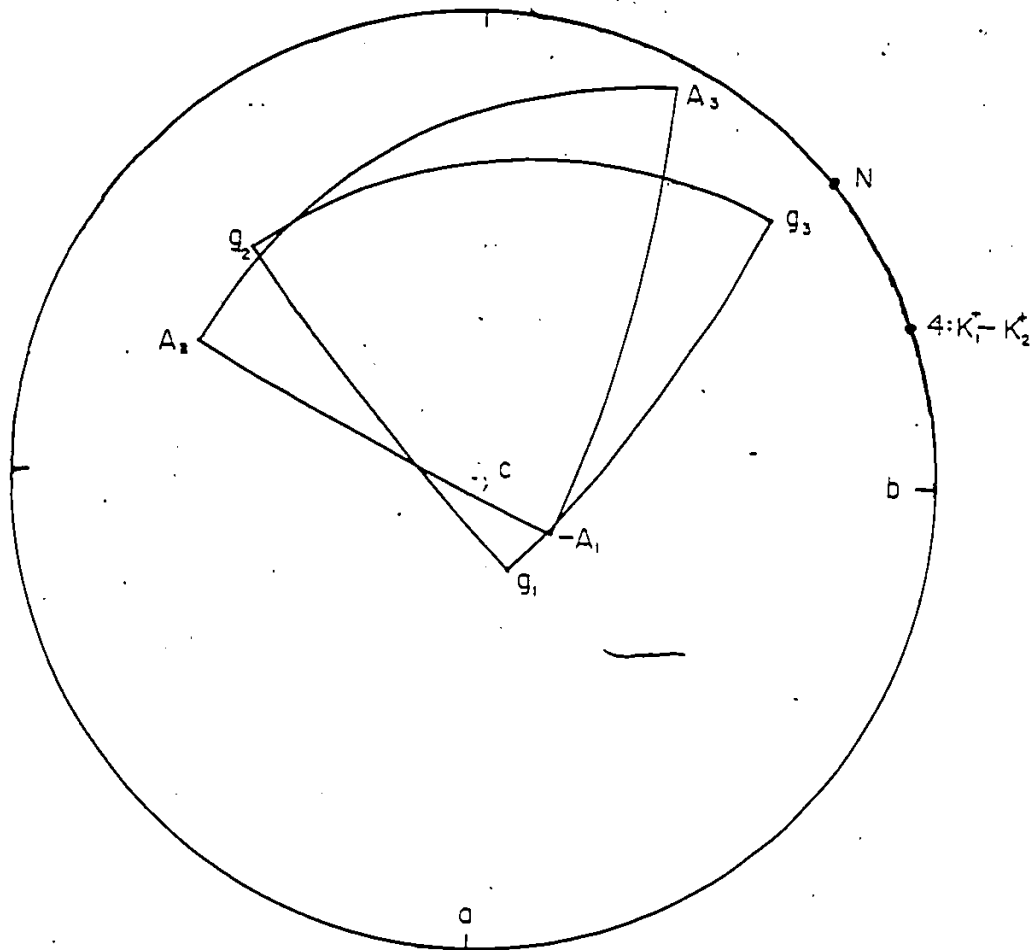


FIG VII.1



Stereogram of principal axes of g and A tensors
with respect to crystallographic axes ,

FIG VII.2

It is generally agreed that g is symmetric in the absence of an external electric field. If we assume that the g and A "tensor" can be adequately fitted by symmetric sets of parameters then g and A can be diagonalized (see appendix 10 for method) to yield the principal axes. These are shown on a stereogram in fig. VII.2 and the principal values tabulated in table VII.2 below. On the stereogram the principal directions of the g and A "tensors" are displayed as points joined by lines of 90° . The stereographic axes are those of the crystal and the line labelled 4 in fig. VII.1 is shown in the ab plane.

TABLE VII.2

g_1	2.122	A_1	55.3
g_2	2.052	A_2	-32.9
g_3	2.407	A_3	241.3
			$(\times 10^{-4} \text{ cm}^{-1})$

As pointed out by Abragam and Bleaney¹¹ g and A are not time second rank tensors, rather gg and AA , however since we are taking both g and A to be symmetric diagonalizing g necessarily diagonalizes gg etc., and so the principal axes and values are unchanged.

As can be seen from the stereogram clear non coincidences in g and A principal axes are observed particularly for g_3 and A_3 . Fair corroboration of Abdulsavirov¹ can be seen with an angle of 22° between direction $K_2^+ - K_1^+ : 4$ and g_3 . Even more significant is the fact that g_3 is within 9° of the nor-

mal to the rectangle formed by the remaining K_1 ligands nearest the vacancy. This is labelled N on the stereogram.

Freeman and Dilbrow² have also investigated $K_2SO_4:Cu^{2+}$ and isostructural $Rb_2SO_4:Cu^{2+}$ and have reported not only noncoincidences in g and A principal axes of 8° but also asymmetries in A. They also cite five other recently reported cases of low symmetry. They only concentrated on centre type 1 as defined by Abdulsabirov¹ (direction 1 and fig. VII.1) and omitted a quadrupole term. However for our set of weak lines $M_I = \pm 1$ transitions varies greatly with direction.

Non-coincidence of g and A tensor is allowed whenever the point symmetry at a paramagnetic ion is monoclinic or triclinic but not for higher symmetries. As fig. VII.2 shows we are clearly dealing here with a case of triclinic symmetry, since non-coincidences in excess of 12° for all axes are clearly demonstrated and there is no common principal axis which would result from monoclinic (C_2) or higher symmetry¹².

As discussed by Belford et al¹², for such low symmetry the A tensor need not be symmetric but the limitation with orientation dependent measurements on single crystals is that A_x , A_y and A_z (XYZ being the principal axis system of the A tensor) along with two Euler angles parameterizing the disposition of gg and AA can be measured, but A has nine independent components so that A cannot be completely characterized. In practical terms this means that even if A is genuinely asymmetric it may not be possible to detect asymmetries.

On a molecular level the problem of the ground state may be very crudely approached by 1st order perturbation theory. It can be shown that a cubic environment with a tetragonal elongation produces the energy level scheme shown below in fig. VII.3.

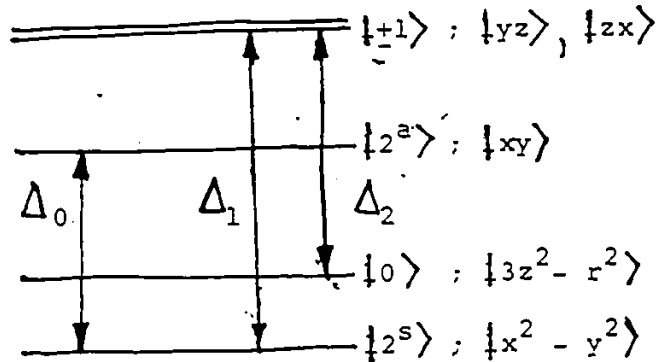


fig. VII.3

Spin orbit coupling cannot mix $|3z^2 - r^2\rangle$ and $|x^2 - y^2\rangle$ but mixes in some of the $|zx\rangle$ and $|xy\rangle$ to give an axial g tensor

$$g_{11} = 2 - \frac{8\lambda}{\Delta_0}$$

$$g_1 = 2 - \frac{2\lambda}{\Delta_1}$$

This is in contrast to a $|3z^2 - r^2\rangle$ ground state which gives

$$g_{11} = 2$$

$$g_1 = 2 - \frac{6\lambda}{\Delta_2}$$

This shows that we are dealing with a predominantly square-planar ground state ie. $|x^2 - y^2\rangle$ in the plane formed by the four coordinating K_1+ sites with the normal N.A low symmetry crystal field however may mix $|x^2 - y^2\rangle$ with $|3z^2 - r^2\rangle$ and

the g values observed can be fitted to a 1st order perturbation expression to give a ground state.

$$|g\rangle = \alpha(|x^2 - y^2\rangle) + \beta(|3z^2 - r^2\rangle)$$

$$\text{with } \beta = 0.065$$

In other words the effect of the vacancy is to mix in $|3z^2 - r^2\rangle$ with z pointing towards the vacancy.

Presumably this centre occurs less frequently for energetic reasons and since the signal is proportional to the concentration of paramagnetic centres this allows a rough estimate of the relative occurrence of the different centre types. This yields an occurrence rate 0.3% that of the other centres which have signals of roughly equal strength.

At any rate the concluding remarks to be made from this investigation are to tentatively confirm the hypothesis of Abdulsabirov¹ and to report a case of Cu^{2+} occupying a low symmetry site resulting in non-coincidences in excess of 12° in $\tilde{g}\tilde{g}$ and $\tilde{A}\tilde{A}$ principal axes.

BIBLIOGRAPHY

1. Abdulsabirov, R.Y., Greznev, Yu. S. and Zoripov, M.M., Soviet Physics - solid State, Vol. 12. No. 2 Aug. 1970.
2. Freeman, T.E. and Pilbrow, J.R., J. Sphy-C: Solid State Vol. 7, 1974.
3. Robinson, F.M.T., J. Phys, Che., 62, 925-928.
4. Zaroyskiy, Ye.K.Zh., EKsp. Teor. Fiz 17, 155, 1947.
5. Griffith, J.S., "The Theory of Transition Metal Ions," Cambridge Univ. Press, 1961.
6. Holuj, F., Can. J. Phys. 46, 287 1968.
7. Froberg, C.E., "Introduction to Numerical Analysis", Addison-Wesley.
8. Ibid., p 111.
9. I.B.M. publication 360A-CM, p 165.
10. Ibid., p 95.
11. Abragam, A. and Bleaney, B., "Electron Paramagnetic Resonance of Transition Ions", Oxford: Clarendon, 1970.
12. Belford, R.L. and Pilbrow, J.R., J. of Mag Res 11, 381-387, 1973.

APPENDIX 1

RESULTS

A right-handed coordinate system was chosen which coincided with the crystallographic axes for tabulation of results and input into the parameter fitting program. Polar coordinates were employed and the correspondence is shown below:

ϕ azimuthal angle

θ polar angle

ϕ	θ	crystallographic axis
0°	0°	b
0°	90°	c
90°	90°	a

Computer printout of results is shown overleaf and the format is as follows

columns 1-4: ϕ

columns 5-8: θ

columns 9-14: ω_{DPPH} MHZ

columns 15-20: transition IF = 1 to JF = 8 MHZ

columns 21-26: transition IF = 2 to JF = 7 MHZ

columns 27-32: transition IF = 3 to JF = 6 MHZ

columns 33-38: transition IF = 4 to JF = 5 MHZ

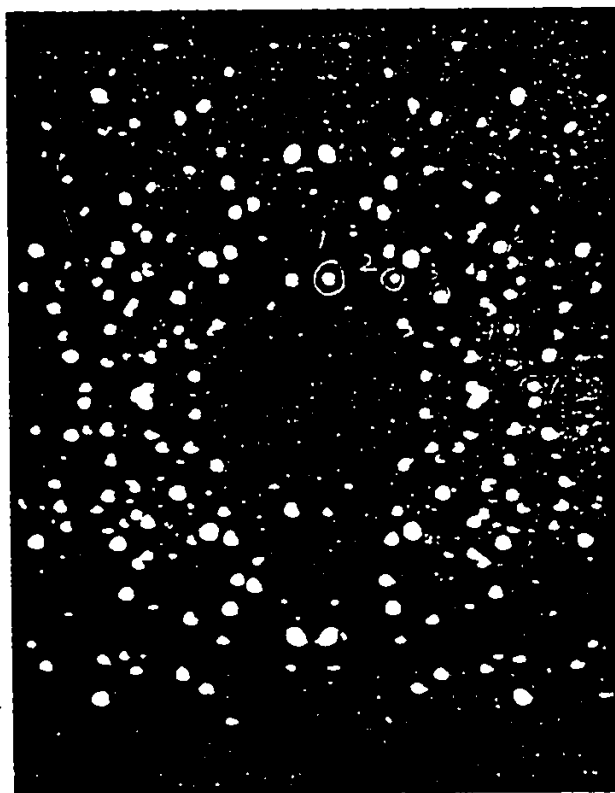
LIST
00003753356654521005479685302245178865
00001004352710071915368421027562480694
00000574374410074986278501037545244547
00000441501223679258035642147756022597
000005773532112574100721143672775251
00000433210774112335720113567740425
000001520135681004110123610143037502
0000144355420112581007080175415720105
00000247395542103689795204157326557254
00001553368755402195336524475320154863
00000204352012257899530215468512773505
00001595362012225048769532105478523662
090004023581075505800137402147099830
09001398361055407310098802143562753018
0900035035210347940244510368785406652
0900297777555310748173215738900234517
0900150353012668754210895820461753324
04970500321054587932015466672214987063
13030900342108769253301455075556149052
04460900342103865912735664000235817334
1354090035875820127174215073003200708
01550900353210407350104215759322100752
16140900352107804780127530100202447369
01550900352104740103173870400103571003
16440900352105687751043286510495727522
01250900352103665075213045667532532158
16750900334588910700532634963735286541
007509003532103659237005142586795322401
1725090032502104477132010883297011451
00250900342101540070923546323701353156
1775090033321017063402153775943253001
00000900320154508670848973002134753654
00000747352201489752451036585792411253
00001057352445479011235740213659575324
0000075335542130830527413585205574158

//
//

APPENDIX 2

IDENTIFICATION OF CRYSTALLOGRAPHIC AXES

X-ray measurements were performed by Dr. M. Khan with the aid of his four circle diffractometer enabling identification of crystallographic axes. The diffractometer used the Syntex system. A photograph of forward scattering spots produced by the sample crystal is shown below.



APPENDIX 3

IV G LEVEL 21

MAIN

DATE = 81181

17/50/CL

C

```

IMPLICIT REAL*8(A-H,C-Z)
COMPLEX*16 DCONJG,DF(36,14),DHT(36,14),EVECT(64),H(36),IMAG,ZERC
1,CA(36),DDP(36),R(36)
DIMENSION A(6),D1F(14),D2F(196),D2FINV(196),EN(8),
1 ALPHA(50),BETA(50),D(14),SIGMA(14),HO(50),IF(11),JF(11),F(12),
2 GNAME(2),DE(14),FDP(50),HEADER(7),P(14),HB(50,11)
DATA C1,C2/'GAUSS',.10-4CM-1'/.IMAG/(0.00,1.00)/,ZEPO/(0.00,0.00)/
    
```

HAMF 40
HAMF 130
HAMF 140

C

INPUT FORMAT STATEMENTS

```

100 FORMAT(2I2,F6.1)
101 FORMAT(2F5.1,3F10.7,2F10.3)
102 FCRMAT(I2,F5.1,I2/7A8,2A8)
103 FCRMAT(8F10.5)
104 FORMAT(16F5.1)
106 FCRMAT (8F10.7)
107 FCRMAT (3F10.7)
108 FCRMAT (5F10.5)
110 FCRMAT(4(8F10.6/),7F10.6/,2(5F10.6/),2F10.6)
111 FCRMAT(1X,12G10.3)
    
```

HAMF 160
HAMF 200
HAMF 210
HAMF 220
HAMF 230
HAMF 240
HAMF 250
HAMF 280

C

OUTPUT FORMAT STATEMENTS

```

150 FCRMAT(1H1, //25X,7A8,2A8)
152 FCRMAT(//1X,'NUMBER OF CRIENTATIONS=',I2,5X,'NUMBER OF ITERATION S',I1//)
154 FCRMAT(//1X,'SIZE OF MATRIX=',I2,5X,'SPIN VALUE=',F6.1,5X,'NUMBER OF PARAMETERS=',I2)
156 FCRMAT(//1X,'DPPH(MHZ)',12F9.4)
158 FCRMAT(//1X,'THETA:',2X,12(F7.1,2X))
160 FCRMAT(//1X,'PHI ',2X,12(F7.1,2X))
162 FCRMAT(//45X,'*** SPECTRA(MHZ) ***')
164 FCRMAT(//10X,12(2X,F7.4))
166 FCRMAT(//1X,'PROTON MHZ TO GAUSS=',F7.3,15X,'DPPH G VALUE=',F8.6,1X,1X,'FREE ELECTRON G VALUE=',F8.6)
168 FCRMAT(1H1, //50X,'ITERATION #',I1//)
169 FCRMAT(14X,'GX',10X,'GY',10X,'GZ',10X,'GXY',9X,'GZX',9X,'GZY')
170 FCRMAT(14X,'AX',10X,'AY',10X,'AZ',10X,'AXY',9X,'AZY')
171 FCRMAT(14X,'QX',10X,'QY',10X,'QZ',10X,'QXY',9X,'QZX',9X,'QZY')
172 FCRMAT(10X,6(2X,F10.5))
174 FCRMAT(//5X,'THETA=',F6.1,5X,'PHI=',F6.1,/)
176 FCRMAT(23X,'TRANSITION',9X,'DEVIATION(GAUSS)')
178 FCRMAT(20X,I2,'/2',2X,'--',2X,I2,'/2',10X,G10.3)
180 FCRMAT(//50X,'PREDICTED DISPLACEMENTS',6X,'D(1)',6X,'D(2)',6X,'D(3)',6X,'D(4)',6X,'D(5)',6X,'D(6)',6X,'D(7)',6X,'D(8)',6X,'D(9)',6X,'D(10)',6X,'D(11)',6X,'D(12)')
181 FCRMAT(2X,12F10.5)
182 FCRMAT(6X,'D(13)',6X,'C(14)',6X,'D(15)',6X,'D(16)',6X,'D(17)',6X,'D(18)')
184 FCRMAT(//50X,'NEW VALUES FOR PARAMETERS')
186 FCRMAT(//50X,'STANDARD DEVIATION FOR EACH PARAMETER')
188 FCRMAT(10X,'VALUE OF',I2,'TH PARAMETER IS NOT CONVERGENT')
190 FCRMAT(//5X,'RMS DEVIATION=',F8.1,' GAUSS',10X,'NEW RMS DEVIATION=',F8.1,' GAUSS',10X,'NUMBER OF LINES=',I3)
    
```

HAMF 290
HAMF 300
HAMF 310
HAMF 320
HAMF 330
HAMF 340
HAMF 350
HAMF 360
HAMF 370
HAMF 380
HAMF 390
HAMF 400
HAMF 410
HAMF 420
HAMF 430
HAMF 450
HAMF 490
HAMF 500
HAMF 510
HAMF 520
HAMF 530
HAMF 540
HAMF 550
HAMF 560
HAMF 570
HAMF 580
HAMF 590
HAMF 660
HAMF 670
HAMF 680

C

READ INPUT DATA CARDS

```

1000 CCNTINUE
READ 100,LN,ITM,TEMP
READ 102,N,SPIN,IMAX,HEACER,GNAME
READ 108,PMHG,GDP,GFE
READ 106,(P(I),I=1,6)
READ 106,(P(I),I=7,IMAX)
READ 100,NCORE
READ 1011,(IF(K),JF(K),K=1,11)
1011 FCRMAT(12(1X,2I1))
PRINT 162
IN=0
10 IN=IN+1
DC 199,K=1,12
159 F(K)=0.0
READ 1030,ALPHA(IN),BETA(IN),HO(IN),(F(K),K=1,10)
1030 FORMAT(6X,2F4.1,12F6.4)
IF(HO(IN).EQ.0.)GOTC30
DC 20,K=1,11
II=IF(K)
    
```

HAMF 690
HAMF 700
HAMF 760

V G LEVEL 21

MAIN

DATE = 81181

17/50/01

```

      JJ=JF(K)
20  HE(IN,K)=F(K)*PMHG
      HOP(IN)=HC(IN)*PMHG*GDF/GFE
      PRINT 2005,IN,ALPHA(IN),BETA(IN),HO(IN),((IF(K),JF(K),F(K),K=1,8)
2005  FCFMAT('0',2X,I3,2F6.1,F7.4,2X,I1(2I1,1X,F7.4))
      GO TO 1C
30  LM=IN-1

```

C
C
C

PRINT INPUT DATA

```

PRINT 150,HEADER,GNAME
PRINT 152,LM,ITN,TEMP
PRINT 154,N,SPIN,IMAX
PRINT 166,PMHG,GDP,GFE

```

HAMF 790
HAMF 800
HAMF 810
HAMF 820
HAMF 830
HAMF 840

C
C
C

DEFINITIONS

```

DR2=DSCFT(2.00)
IMAX2=IMAX*IMAX
NN=(N+1)*N/2

```

HAMF 920
HAMF 930
HAMF 940
HAMF 950
HAMF 960
HAMF 970
HAMF 980
HAMF 99

C
C
C
C
C

CORRECT AND CONVERT FIELD VALUES

ITERATIONS LOOP STARTS HERE

```

DC 204 IT=1,ITM
NL=0

```

HAMF 1000
HAMF 1100
HAMF 1110
HAMF 1120
HAMF 1130
HAMF 1140
HAMF 1150
HAMF 1160
HAMF 1170

C
C
C

INITIALIZATION

```

XLSF=0.00
DC 207 IJ=1,NN
F(IJ)=ZERO
B(IJ)=ZERO
DA(IJ)=ZERO
DOP(IJ)=ZERO
DO 207 J=1,IMAX
DH(IJ,J)=ZERO
207 DHT(IJ,J)=ZERO
DO 206 IJ=1,IMAX2
206 D2F(IJ)=0.00
DC 208 I=1,IMAX
208 D1F(I)=0.00
PRINT 168,IT
PRINT 169
PRINT 172.(P(I),I=1,6)
PRINT 170
PRINT 172.(P(I),I=7,12)
PRINT 171
PRINT 172.(P(I),I=13,14)

```

HAMF 1180
HAMF 1190
HAMF 1200
HAMF 1210
HAMF 1280

C ***** QUADRUPLE TERM *****

```

DC 402 LL=1,2
NL=12+LL

```

```

402 A(LL)=F(NL)
CALL QUAD(B,A)
DC 404 LL=1,2
DC 406 LO=1,2

```

```

406 A(LO)=0.00
A(LL)=1.00
CALL QUAD(DA,A)
NX=12+LL
DC 408 NA=1,36

```

```

408 CH(NA,NX)=DA(NA)
404 CCNTINUE

```

C \$\$\$\$\$\$ SHFS TERM \$\$\$\$\$\$

```

DC 403 LL=1,6
NL=6+LL

```

```

403 A(LL)=P(NL)
CALL SHFS(DA,A)
DO 430 LL=1,36

```

```

430 B(LL)=B(LL)+DA(LL)
DO 405 LL=1,6
DC 407 LO=1,6

```

```

407 A(LO)=0.00
A(LL)=1.00
CALL SHFS(DA,A)
DC 409 NA=1,36
NX=6+LL

```

```

409 DH(NA,NX)=DA(NA)
405 CCNTINUE

```

C
C
C
C
C
C
C
C
C

```

      SETTING UP FIELD INDEPENDENT COMPONENTS OF MATRIX ELEMENTS OF H(IAB) AND FIELD INDEPENDENT MATRIX ELEMENTS OF DH(IAB,NX)
      SETUP THE A-MATRIX

```

```

      TRANSITIONS LOOP STARTS HERE
      CALCULATE ENERGY DIFFERENCE FROM EXPERIMENTAL FREQUENCY
      CALCULATE COMPONENTS OF FIELD VALUES

```

```

DO 222 L=1,LM
  THETAM = BETA(L) *.0174533
  PHIM = ALPHA(L) *.0174533
  SINTH=DSIN(THETAM)
  COSTH=DCOS(THETAM)
  SINPH=DSIN(PHIM)
  COSPH=DCOS(PHIM)
  X=COSPH*SINTH
  Y=SINPH*SINTH
  Z=COSTH
  PRINT 174, BETA(L),ALPHA(L)
  PRINT 175

```

```

303 NY=0
DO 223 INDEX=1,11
  IF(HR(L,INDEX).LE.0.) GO TO 246
  HX=HR(L,INDEX)*X
  HY=HR(L,INDEX)*Y
  HZ=HR(L,INDEX)*Z
  NL=NL+1

```

C
C
C

```

      SETTING UP FIELD DEPENDENT MATRIX ELEMENTS OF H(IAB)

```

```

DO 410 LL=1,6
410 A(LL)=0(LL)
  CALL MHAM(A,DA,HX,HY,HZ)
  DO 409 LL=1,6
450 F(LL)=DA(LL)+R(LL)
  SET-UP THE DERIVATIVES OF THE G-MATRIX
  DO 412 LL=1,6
  DO 414 LOT=1,6
414 A(LOT)=0.00
  A(LL)=1.00
  CALL MHAM(A,DA,HX,HY,HZ)
  DO 410 NH=1,36
416 DH(NH,LL)=DA(NH)
412 CONTINUE

```

C
C
C
C

```

      CALL CEIGEN DIAGONALIZE COMPLEX MATRIX H(IAB)
      OBTAIN EIGEN VALUES STORED DIAGONALLY IN H(IAB)
      OBTAIN EIGENVECTORS STORED IN ETECT(IE)

```

```

2500 FORMAT(9(2X,112.5))
  MV=0
  CALL CEIGEN(H,ETECT,N,MV)
  DO 236 K=1,N
  IAB=K*(K+1)/2
  EN(K)=H(IAB) / 2.00229
  KW=IF(INDEX)
  KK=JF(INDEX)
  DELTA=(EN(KK)-EN(KW))-HDP(LL)
  M=IF(INDEX)
  K=JF(INDEX)
  PRINT 179,M,K,DELTA

```

C
C
C
C

```

      TRANSFORM DH(IAB,I) TO NEW BASIS

```

```

704 NY=1
DO 240 I=1,IMAX
DO 451 I2=1,36
451 DA(I2)=DH(I2,I)
  CALL STC(CD,DA,ETECT,N,KW,KN)
  DO 450 I2=1,36
450 DHT(I2,I)=DHP(I2)
240 CONTINUE
  XLSF=XLSF+(DELTA*K)

```


APPENDIX 5

56

V G LEVEL 01

MAIN

DATE = 81176

22/01/58

```

405 DH(NA,IX)=DA(NA)
405 CONTINUE
                                HAMF1310
                                SHAMF1320
                                HAMF1330
                                SETTING UP FIELD INDEPENDENT COMPONENTS OF MATRIX ELEMENTS OF H(IAB) AND FIELD INDEPENDENT MATRIX ELEMENTS OF DH(IAB)
                                SET-UP THE A-MATRIX
                                HAMF1340
                                TRANSITIONS LOOP STARTS HERE
                                HAMF1710
                                HAMF1720
                                CALCULATE ENERGY DIFFERENCE FROM EXPERIMENTAL FREQUENCY
                                HAMF1730
                                CALCULATE COMPONENTS OF FIELD VALUES
                                HAMF1740
                                HAMF1750
                                HAMF1760

DO 222 L=1,LM
THETAM = BETA(L) *.0174533
PHIVE ALPHA(L)*.0174533
SINTH=OSIN(THETAM)
COSTH=OCOS(THETAM)
SINPH=OSIN(PHIM)
COSPH=OCOS(PHIM)
Y=COSPH*SINTH
Z=SINPH*SINTH
W=COSTH
IF (.NOT. ITW) GO TO 303
PRINT 174, BETA(L),ALPHA(L)
PRINT 176
                                HAMF1900

303 NY=0
DO 222 INDEX=1,11
IF (HR(L,INDEX).LE.0.) GO TO 248
HX=HR(L,INDEX)*X
HY=HR(L,INDEX)*Y
HZ=H(L,INDEX)*Z
NL=NL+1
                                HAMF1930
                                HAMF1970
                                HAMF1980
                                HAMF1990
                                SETTING UP FIELD DEPENDENT MATRIX ELEMENTS OF H(IAB)

DO 410 LL=1,6
410 A(LL)=D(LL)
CALL MHAM(A,DA,HX,HY,HZ)
DO 409 LL=1,6
409 H(LL)=DA(LL)+H(LL)
                                SET-UP THE DERIVATIVES OF THE G-MATRIX
DO 412 LL=1,6
DO 414 LCT=1,6
414 A(LCT)=0.00
A(LL)=1.00
CALL MHAM(A,DA,HX,HY,HZ)
DO 416 NH=1,30
416 H(NH,LL)=DA(NH)
412 CONTINUE
                                HAMF2340
                                HAMF2350
                                HAMF2360
                                HAMF2370
                                HAMF2380
                                CALL CEIGEN DIAGONALIZE COMPLEX MATRIX H(IAB)
                                OBTAIN EIGEN VALUES STORED DIAGONALLY IN H(IAB)
                                OBTAIN EIGENVECTORS STORED IN EVECT(IE)

2500 FFORMAT(F(2X,112.5))
MV=0
CALL CEIGEN (H,EVECT,N,MV)
DO 235 K=1,N
IAB=K*(K+1)/2
                                HAMF2430
                                HAMF2440
                                235 EN(K)=H(IAB) /2.00229
                                KX=IF(INDEX)
                                KY=IF(INDEX)
                                KZ=IF(INDEX)
                                DELTA=(EN(NK)-EN(KX))-HCF(L)
                                Y=IF(INDEX)
                                X=IF(INDEX)
                                IF (.NOT. ITW) GO TO 304
                                PRINT 176,M,K,DELTA
                                HAMF2550

                                TRANSFORM DH(IAB,I) TO NEW BASIS
                                HAMF2560
                                HAMF2570
                                HAMF2580

204 M=1
DO 451 I=1, IMAX
DO 451 J=1, 30
451 DA(I,J)=DH(I,J)
CALL STCM(DA,DA,EVECT,N,KW,NK)
DO 452 I=1, 24
452 DH(I,J)=DDH(I,J)

```

V G LEVEL 21

MAIN

DATE = 81176

22/01/88

```

240 CONTINUE
XLSE=XLSF+(DELTA**2)
-----HAMF2750

                SETTING UP DE(INDEX,I)
                -----
                KAV=(KV*PK+KW)/2
                KAV=K*(K+1)/2
                DO 246 I=1,IMAX
                DE(I)=DHT(KAV,I)-DHT(KK,I)
                -----
                SETTING UP DIF/DP(I)
                -----
                DIF(I)=DIF(I)+(2*DELTA*DE(I))
246 CONTINUE
248 CONTINUE
                SETTING UP D2F/DF(I)DP(J)
                -----
                DO 250 I=1,IMAX
                DO 250 J=1,IMAX
                IF(LE(L,INDEX).LE.0.0) GO TO 222
                IJ=I+(J-1)*IMAX
                DCF=0.00
                DO 252 ID=1,N
                IF(ID.LT.KW) GO TO 256
                IF(ID.GT.KW) GO TO 256
                KID=KW+(ID-ID-ID)/2
                DHTI=D(CONJG(DHT(KID,I)))
                DHTJ=DHT(KID,J)
                IF(ID.LT.NK) GO TO 260
                IF(ID.LT.NK) GO TO 256
                NICA=N+(ID-ID-ID)/2
                DHTIA=D(CONJG(DHT(KIDA,I)))
                DHTJA=DHT(KIDA,J)
                GO TO 262
254 KID=ID+(K*KK-K)/2
                DHTI=DHT(KID,I)
                DHTJ=D(CONJG(DHT(KID,J)))
                KIDA=ID+(N*NK-N)/2
                DHTIA=DHT(KIDA,I)
                DHTJA=D(CONJG(DHT(KIDA,J)))
                GO TO 262
258 KIDA=ID+(N*NK-NK)/2
                DHTIA=DHT(KIDA,I)
                DHTJA=D(CONJG(DHT(KIDA,J)))
                D2F=D2F+2.00*(DHTIA*DHTJA/(EN(NK)-EN(ID))
                GO TO 262
260 D2F=D2F-2.00*(DHTI*DHTJ/(EN(KW)-EN(ID)))
                GO TO 262
262 D2F=D2F+2.00*(DHTIA*DHTJA/(EN(NK)-EN(ID))-2.00*(DHTI*DHTJ/
                (EN(KW)-EN(ID)))
264 CONTINUE
                DIF(IJ)=DIF(IJ)+(2.00*DE(I)*DE(J))+D2F*DELTA
266 CONTINUE
268 CONTINUE
                NFREC=NL-IMAX
                XLSF=XLSF/NFREC
                DO 264 I=1,IMAX
                DIF(I)=DIF(I)/NFREC
                DO 264 J=1,IMAX
                IJ=I+(J-1)*IMAX
                D2F(IJ)=D2F(IJ)/NFREC
                DIF INV(IJ)=D2F(IJ)
264 CONTINUE
                -----
                CALCULATE AND PRINT PREDICTED DISPLACEMENTS D(I)
                PRINT 2000, (D2F INV(IJ),IJ=1,IMAX2)
                PRINT 3000, (DIF(I),I=1,IMAX)
                -----
                CALL DIF INV(D2F INV,IMAX,DELTA)
                PRINT 1000, (D(X,14),X=1)
2000 DO 200 I=1,IMAX
                IJ=I*IMAX
                D(I)=0.00
                DO 200 J=1,IMAX
                IJ=IJ+IMAX

```

HAMF2760
 HAMF2770
 HAMF2780
 HAMF2800
 HAMF2805
 HAMF2810
 HAMF2820
 HAMF2830
 HAMF2840
 HAMF2850
 HAMF2860
 HAMF2870
 HAMF2880
 HAMF2890
 HAMF2900
 HAMF2910
 HAMF2920
 HAMF2930
 HAMF2950
 HAMF2960
 HAMF2970
 HAMF2980
 HAMF2990
 HAMF3000
 HAMF3010
 HAMF3020
 HAMF3030
 HAMF3040
 HAMF3050
 HAMF3060
 HAMF3070
 HAMF3080
 HAMF3090
 HAMF3100
 HAMF3110
 HAMF3120
 HAMF3130
 HAMF3140
 HAMF3150
 HAMF3160
 HAMF3170
 HAMF3180
 HAMF3190
 HAMF3200
 HAMF3210
 HAMF3220
 HAMF3230
 HAMF3240
 HAMF3250
 HAMF3260
 HAMF3270
 HAMF3280
 HAMF3290
 HAMF3300
 HAMF3310
 HAMF3320
 HAMF3330
 HAMF3340
 HAMF3350
 HAMF3360
 HAMF3370
 HAMF3380
 HAMF3390
 HAMF3400
 HAMF3410
 HAMF3420
 HAMF3430
 HAMF3440
 HAMF3450
 HAMF3460

V G LEVEL 21

MAIN

DATE = 81176

22/01/83

```

260 D(I)=D(I)-D2F(INV(IJ))*DIF(J)
PRINT 180
PRINT 181,(D(I),I=1,12)
PRINT 182
PRINT 181,(D(I),I=12,IMAX)
C
C          CALCULATE AND PRINT NEW VALUES FOR PARAMETERS P(I)
C
DO 265 I=1,IMAX
265 P(I)=P(I)+D(I)
PRINT 184
PRINT 185
PRINT 172,(P(I),I=1,6)
PRINT 170
PRINT 172,(P(I),I=7,12)
PRINT 171
PRINT 172,(P(I),I=13,14)
XLSNEW=XLSF
II=-IMAX
DO 270 I=1,IMAX
II=II+IMAX+1
XLSNEW=XLSNEW+DIF(I)*D(I)+(D2F(II)*D(I)*D(I))/2.00
JMIN=I+1
IF(I.GE.IMAX) GO TO 270
DO 272 J=JMIN,IMAX
IJ=II-I+J
XLSNEW=XLSNEW+D2F(IJ)*D(I)*D(J)
272 CONTINUE
270 CONTINUE
C
C          CHECK FOR CONVERGENCE OF P(I)
C
II=-IMAX
DO 274 I=1,IMAX
II=II+IMAX+1
IF (D2F(II).LT.0.00) PRINT 188,I
C
C          CALCULATE SIGMA(I)
C
274 SIGMA(I)=DSORT(DAPS(D2F(INV(II))*XLSNEW*2.00/NFREE))
DMS=DSORT(XLSF)
RMSNEW=DSORT(XLSNEW)
PRINT 186
PRINT 189
PRINT 172,(SIGMA(I),I=1,6)
PRINT 170
PRINT 172,(SIGMA(I),I=7,12)
PRINT 171
PRINT 172,(SIGMA(I),I=13,14)
PRINT 190,RMS,RMSNEW,NL
294 CONTINUE
IF (NCRIT) 1000,1001,1000
1001 CONTINUE
STOP
END

```

HAMF3470
HAMF3480
HAMF3490HAMF3500
HAMF3510
HAMF3520
HAMF3530
HAMF3540
HAMF3550HAMF3580
HAMF3590
HAMF3600
HAMF3610
HAMF3620
HAMF3630
HAMF3640
HAMF3650
HAMF3660
HAMF3670
HAMF3680
HAMF3690
HAMF3700
HAMF3710
HAMF3720
HAMF3730
HAMF3740
HAMF3750
HAMF3760
HAMF3770
HAMF3780
HAMF3790
HAMF3800
HAMF3810
HAMF3820
HAMF3830HAMF3850
HAMF3860HAMF4200
HAMF4210

Subroutine: CEIGEN

Purpose: Compute eigenvalues and eigenvectors of a Hermitean matrix (double precision complex).

Usage: CALL CEIGEN (A,R,N,MV).

Description of parameters:

A - (COMPLEX * 16) original Hermitean matrix, destroyed during computation. Upon return, A is the diagonalized matrix with storage is used; the upper right side of the matrix actually stores: the (I,J) element is the $I + (J * J - J)/2$ element of A for $I \leq J$. For $I > J$ the (I,J) element is the complex conjugate of the (J,I) element, i.e. of the $J + (I * I - I)/2$ member of A.

R - (COMPLEX * 16) the unitary transformation which diagonalizes A. The columns of R are eigenvectors of A ordered as are the eigenvalues.

N - the order (dimension) of A and R

MV - input code:

0 compute eigenvalues and eigenvectors
 1 compute eigenvalues only. (R need not be dimensioned but must still appear in calling sequence.)

Method: an extension of the Jacobi method to Hermitean matrices as given, for example in C.-E Froberg, Introduction to Numerical Analysis (Addison-Wesley, 1965) p. 111. The coding parallels that for EIGEN (see publication 360A-CM, p. 165).

Programmed by: Wm. E. Bavlis,
 Physics Department,
 University of Windsor.

Execution time: 0.5 sec CPU on the IBM 360 Model 50 of University of Windsor for $N = 4$. The time will vary roughly as N^4 but will be less if some off-diagonal elements of A are initially = 0.

```

$JOB LIST XXXXXXXXXXXX UNWIN
C COMPUTES DOUBLE PRECISION EIGENVALUES AND, UNLESS MV=1, ALSO COMPLEX EIGENVECTORS OF THE HERMITEAN MATRIX CA OF DIMENSION N. THE JACobi METHOD IS USED.
C
C THE CALLING PARAMETERS ARE
C CA - THE HERMITEAN MATRIX TO BE DIAGONALIZED. COMPACT STORAGE IS USED. NAMELY THE (I,J)TH ELEMENT OF THE UPPER RIGHT HALF OF THE HERMITEAN MATRIX IS ELEMENT I+(J*J-J)/2 OF CA.
C UPON RETURN, CA IS DIAGONALIZED WITH THE EIGENVALUES IN ASCENDING ORDER ON THE DIAGONAL.
C CR - THE INPUT VALUES OF THIS MATRIX ARE NOT USED. UPON RETURN, IF MV.NE. 1, CR CONTAINS THE COMPLEX EIGENVECTORS OF THE INPUT CA MATRIX. THE EIGENVECTORS ARE STORED COLUMNWISE IN THE SAME SEQUENCE AS THE EIGENVALUES.
C N - THE DIMENSION OF THE MATRIX TO BE DIAGONALIZED.
C MV - IF EQUAL TO 1, ONLY EIGENVALUES AND NOT EIGENVECTORS ARE COMPUTED.
C
C W. E. BAYLIS, PHYSICS, U. WINDSOR, WINDSOR, ONTARIO, FEB. 1972
C
C IMPLICIT REAL*8 (A,D,G,O-Z), COMPLEX*16(C)
C COMPLEX*16 ONE/(1.0D0,0.0D0)/, ZERO/(0.0D0,0.0D0)/
C COMPLEX*16 DCCNJG
C REAL*8 CDABS
C REAL*8 COSP,COSP2
C DIMENSION CA(1),CS(1),CSINP(2)
C
C CHECK DIMENSION
C
C IF(N-1)1,2,5
C 1 PRINT 200,N
C 200 FORMAT(' ERROR. ATTEMPT TO DIMENSION CEIGEN BY N>.16..'/) STOP
C EXECUTION.'
C STOP
C 2 IF(MV.EQ. 1) GO TO 4
C CR(1) = ONE
C 4 RETURN
C
C GENERATE IDENTITY MATRIX
C
C 5 RANGE = 1.0D-12
C IF(MV.EQ. 1) GO TO 25
C IQ = -N
C DO 20 J=1,N
C IQ = IQ + N
C DO 20 I=1,N
C IJ = IQ + I
C CR(IJ) = ZERO
C IF(I.EQ. J) CR(IJ) = ONE
C 20 CONTINUE
C
C COMPUTE INITIAL AND FINAL NORMS
C
C 25 ANORM = 0.0D0
C Y = 0.0D0
C IJ = 0
C DO 35 J=1,N
C DO 35 I=1,J
C IJ = IJ + 1
C X = CA(IJ)*DCCNJG(CA(IJ))
C ANCRM = ANCRM + X
C IF(I.EQ. J) GO TO 35
C Y = Y + X
C 35 CONTINUE
C ANORM = 1.414D0*DSQRT(ANORM)
C ANRMX = ANCRM*RANGE/DFLOAT(N)
C IF(Y.LE. ANRMX) GO TO 165
C
C INITIALIZE INDICATORS AND COMPUTE THRESHOLD. :THR:
C
C IND = 0
C THR = ANORM
C 45 THR = THR/DFLOAT(N)
C 50 L=1
C 55 M=L+1
C LO = (L*L-L)/2
C LL = LC + L

```

00004300
00004400
00004500
00004600
00004700
00004800
00004900
00005000
00005100
00005200
00005300
00005400
00005500
00005600
00005700
00005800
00005900
00006000
00006100
00006200
00006300
00006400
00006500
00006600
00006700
00006800
00006900
00007000
00007100
00007200
00007300
00007400
00007500
00007600
00007700
00007900
00007900
00007900
00008000
00008100
00008200
00008300
00008400
00008500
00008600
00008700
00008800
00008900
00009000
00009100
00009200
00009300
00009400
00009500
00009600
00009700
00009800
00009900
00010000
00010100
00010200
00010300
00010400
00010500
00010600
00010700
00010800
00010900
00011000
00011100
00011200
00011300
00011400
00011500
00011600
00011700
00011800
00011900

```

ILO = N*(L-1)
60 MJ = (M*M-M)/2
LM = L + MQ

```

COMPUTE ELEMENTS OF 2X2 ROTATION MATRIX IF OFF-DIAGONAL ELEMENT IS LARGER THAN THR

```

GAM = CDABS(CA(LM))
IF(GAM .LT. THR) GO TO 130
MM = MQ + M
IMO = N*(M-1)
IND = 1
X = CA(LM)
IF(X .LT. 0.0D0) GAM = -GAM
X = (CA(LL) - CA(MM))/2.0D0
Y = GAM/DSORT(X*X+GAM*GAM)
IF(X .LT. 0.0D0) Y = -Y
SINP = X/DSORT(2.0D0*(1.0D0 + CSORT(1.0D0 - Y*Y)))
SINP2 = SINP*SINP
COSPP2 = 1.0D0 - SINP2
COSP = DSORT(COSP2)
CSINP(1) = GAM*SINP/CA(LM)
CSINP(2) = DCCNJG(CSINP(1))
GSIN2P = 2.0D0*GAM*SINP*COSP

```

ROTATE COLUMNS AND ROWS L AND M

```

IQ = 0
DO 125 I=1,N
IQ = IC + I - 1
IF(I-M) 85,115,90
85 IM = I + MQ
MCONJ = 1
IF(I-L) 100,115,105
100 IL = I + LQ
LCCNJ = 1
GO TO 110
90 IM = M + IQ
MCCNJ = 2
105 IL = L + IQ
LCCNJ = 2
110 CX = CA(IM)*CSINP(MCONJ)
CY = CA(IL)*CSINP(3-LCCNJ)
IF(MCONJ .EQ. LCCNJ) GO TO 112
CA(IL) = CA(IL)*CCSP + LCCNJG(CX)
CA(IM) = CA(IM)*CCSP - MCCNJG(CY)
GO TO 115
112 CA(IL) = CA(IL)*COSP + CX
CA(IM) = CA(IM)*COSP - CY
115 IF(MV .EQ. 1) GO TO 125
ILR = ILO + I
IMR = IMO + I
CX = CR(ILR)*COSP + CR(IMR)*CSINP(1)
CR(IMR) = CR(IMR)*COSP - CR(ILR)*CSINP(2)
CR(ILR) = CX
125 CCNTINUE
X = CA(LL)*SINP2 + CA(MM)*COSP2 - GSIN2P
CA(LL) = CA(MM)*SINP2 + CA(LL)*COSP2 + GSIN2P
CA(MM) = X
CA(LM) = ZERO
130 IF(M .EQ. N) GO TO 140
M = M+1
GO TO 60
140 IF(L .EQ. N-1) GO TO 150
L = L+1
GO TO 55
150 IF(IND .EQ. 0) GO TO 150
IND = 0
GO TO 50
160 IF(THR .GT. ANPMX) GO TO 45

```

SORT EIGENVALUES AND EIGENVECTORS

```

165 IO = -N
LL=0
JC 185 I = 1,N
IQ = IC + N
LL = LL + I
JO = N*(I-2)
X = CA(LL)

```

- 00012000
- 00012100
- 00012200
- 00012300
- 00012400
- 00012500
- 00012600
- 00012700
- 00012800
- 00012900
- 00013000
- 00013100
- 00013200
- 00013300
- 00013400
- 00013500
- 00013600
- 00013700
- 00013800
- 00013900
- 00014000
- 00014100
- 00014200
- 00014300
- 00014400
- 00014500
- 00014600
- 00014700
- 00014800
- 00014900
- 00015000
- 00015100
- 00015200
- 00015300
- 00015400
- 00015500
- 00015600
- 00015700
- 00015800
- 00015900
- 00016000
- 00016100
- 00016200
- 00016300
- 00016400
- 00016500
- 00016600
- 00016700
- 00016800
- 00016900
- 00017000
- 00017100
- 00017200
- 00017300
- 00017400
- 00017500
- 00017600
- 00017700
- 00017800
- 00017900
- 00018000
- 00018100
- 00018200
- 00018300
- 00018400
- 00018500
- 00018600
- 00018700
- 00018800
- 00018900
- 00019000
- 00019100
- 00019200
- 00019300
- 00019400
- 00019500
- 00019600
- 00019700
- 00019800
- 00019900

```

DD 185 J=I,N
JO = JC + N
MM = (J*J+J)/2
Y = CA(MM)
IF(X .LE. Y) GO TO 185
CA(LL) = Y
CA(MM) = X
X = Y
IF(MV .EQ. 1) GO TO 185
DO 180 K=1,N
ILR = IQ + K
IMR = JO + K
CX = CR(ILR)
CR(ILR) = CR(IMR)
180 CR(IMR) = CX
185 CONTINUE
RETURN
END

```

```

00020000
00020100
00020200
00020300
00020400
00020500
00020600
00020700
00020800
00020900
00021000
00021100
00021200
00021300
00021400
00021500
00021600
00021700

```

//

APPENDIX 7

64

```

$JOB  LIST  XXXXXXXXXXX UNW IN
1  SUBROUTINE DGMPRC(A,B,R,N,M,L)
2  IMPLICIT REAL(A-H,O-Z)
3  DIMENSION A(144),E(144),R(144)
4  IR=0.DC
5  IK=-M
6  DO 10 K=1,L
7  IK=IK+M
8  DO 10 J=1,N
9  IR=IR+1
10  JI=J-N
11  IB=IK
12  R(IR)=0.DC
13  DO 10 I=1,M
14  JI=JI+N
15  IB=IB+1
16 10 R(IR)=R(IR)+A(JI)*B(IB)
17  RETURN
18  END
//

```

```

//W  JOB  (U102005538),CLASS=W
//W  JCB  (U102005538),CLASS=W

```

```

JOB 787
JOB 787

```


APPENDIX 8

DIAGONALIZATION OF g and A TENSORS

The computer program used to evaluate the principal axes and values of the g and A tensors is shown overleaf. The program forms a traceless tensor and then employs three rotations to diagonalize this tensor.

VITA AUCTORIS

I was born in Loughborough, Leicestershire, in 1959. I completed my secondary education at Hind Leys College Shepsled and Burleigh Community College Loughborough. I graduated from Queens' College in the University of Cambridge in 1980 with a B.A. in Physics. At present I am completing requirements towards my MSc at the University of Windsor, Ontario.

PAGE 67 MISSING